U.S. Department of the Interior

U.S. Geological Survey

GEOPHYSICAL LOGS AND GROUNDWATER CHEMISTRY IN THE A/M AREA, INTERIM REPORT, SAVANNAH RIVER SITE, SOUTH CAROLINA

Philip H. Nelson[1] and Joyce E. Kibler[1]

Open-File Report 95-507

This report is preliminary and has not been reviewed for conformity with U.S. Geological Survey editorial standards. Any use of trade names is for descriptive purposes only and does not imply endorsement by the USGS. This work was supported by the Department of Energy under Interagency Agreement DE-AI09-91 SR18222.

1995

1. U.S. Geological Survey
Denver, Colorado

TABLE OF CONTENTS

List of Tables

List of Figures

SUMMARY

Subsurface data from the A/M area, comprised of water sample analyses, physical property data from laboratory measurements, and borehole logs have been compiled and examined. Our objectives are to support concurrent cross-hole geophysical studies, to use the logs in determining properties bearing upon contaminant transport in the subsurface, and to improve geological correlations by gaining a better understanding of log response. This report documents our findings on groundwater chemistry and core-related properties, our compilation of geophysical logs and penetrometer runs into a coherent data base, and a computational scheme for estimating porosity and water content as a function of depth in the vadose zone.

Groundwater conductivity in the A/M area varies from 20 to 3000 μS/cm. Two types of contamination have added solute and increased the conductivity of natural groundwater which is inherently quite fresh. Samples with conductivity exceeding 300 μS/cm are characterized by high pH, sulfate in excess of 10 ppm, and sodium exceeding 20 ppm. These high conductivity, high pH samples contacted and leached grout in the wellbore annulus and occur in only a few wells. Samples with conductivity less than 300 μS/cm have low pH and nitrate concentrations ranging from near zero to 25 mg/L. The nitrate ion is attributed to salt solutions codisposed with chlorinated hydrocarbon in the M-area settling basin. In wells west and south of the settling basin, high nitrate often occurs with high chlorinated hydrocarbons.

Geophysical and cone penetrometer logs from the A/M area were compiled into a data base: stress and resistivity logs from 27 penetrometer runs, gamma ray from 9 cased MSB-series holes, gamma ray and electrical from 30 open holes, and gamma ray, neutron, density, and electrical from 10 open holes. Examination of laboratory measurements of core samples showed that average porosity is 0.39, average grain density is 2.63 g/cm^3, kaolinite is the dominant clay mineral, and that minimum water saturation can be expected to be around 0.4.

Logs from the MHT-series of holes, collected during the Integrated Demonstration Program and comprising the most complete set of logs, were evaluated in detail. Borehole corrections and smoothing filters were applied to the neutron, density, gamma-ray, and electrical logs. Partially saturated sands can be recognized from combinations of the neutron and density logs or from resistivity and density logs. Porosity and saturation were calculated from the density and resistivity log, and a clay flag from the neutron and resistivity logs.

The calculated logs suggest a three-way partition of vadose zone lithologies into clay-rich, high-silt/low-clay, and partially saturated sand zones. Clay-rich zones are delineated by low resistivity and/or high neutron porosity. High-silt/low-clay zones occur where resistivity values are moderate and where the rock is saturated or nearly so. Partially saturated sand occurs where saturation is less than 1, that is, where moisture content is less than vadose-zone porosity. This three-way division of the vadose zone is believed to be important in terms of contaminant, water, and gas transport.

Regarding future log acquisition, we recommend that the standard logging suite be upgraded

to include a guard or focused resistivity, a neutron, and a density log. In terms of existing data, we recommend that analysis of existing logs be completed and that the results be interpreted cooperatively with personnel knowledgable regarding the stratigraphy and mineralogy. The primary work to be done on existing logs is to derive true formation resistivity from long and short normal resisitivity logs, in order to sharpen formation boundaries and delineate conductive zones. The goals of a final interpretation are two-fold: to ascertain whether low resistivity registrations below water table are due to conductive groundwater and to incorporate the physical property information available from logs into a correlation of flow units.

INTRODUCTION

The A/M area at the Savannah River Site is currently undergoing characterization and pilot remediation work to locate and recover chlorinated solvents which were released to the subsurface. As part of this characterization effort, subsurface measurements have been obtained by sampling water and core retrieved from wells, by geophysical logging of boreholes, and by cone penetrometer runs. This report describes the first phase of a synthesis of the existing geophysical logs and penetrometer runs; no new data were obtained under this activity.

The sequence of Late Cretaceous and Tertiary fluvial/deltaic to shallow marine sediments have been divided into four hydrogeological units (Figure 1). The vadose zone extends from surface to the water table at approximately 150 feet subsurface. Screened intervals sampling the aquifers are also shown in Figure 1. The 'tan clay' represents a major hydrological barrier within the vadose zone, while the 'green clay' separates the M-area from the Lost Lake aquifer. Nomenclature relating hydrogeologic nomenclature, well screen designations, and hydrogeologic symbols are given in Table 1.

Table 1. Relationship between hydrogeologic symbols, older hydrogeologic nomenclature, and screen designations. Screen labels are the ones usually, but not always, set within a given aquifer or confining zone.

Hydrogeologic name and symbols	Older hydrogeologic name	Usual screen label
M-area aquifer: M, GCL, MGCL, MGC	W.T.	D, E
Lost Lake aquifer: UL, LL, L(UD), LL/CBC	lower and upper Congaree	B, C
Crouch Branch confining zone: MCBC	Ellenton Sand	A
Crouch Branch aquifer: CBA	Black Creek	TA, TB

Our objectives in examining the borehole data are to support concurrent cross-hole geophysical studies by colleagues at the USGS (Ellefsen, 1995), to use the logs in determining properties bearing upon contaminant storage and transport in the subsurface, and to improve geological correlations by gaining a better understanding of log response. This report documents our findings on groundwater chemistry and core-related properties, our compilation of much of the data available from the A/M area into a coherent data base, and a computational scheme for estimating porosity and water content as a function of depth in the vadose zone. These activities have enabled us to support the cross-hole work, and have greatly improved our understanding of water chemistry and rock properties within the A/M area. The compilation of data is necessary preparation for correlation work, which has not yet commenced.

GROUNDWATER CHEMISTRY

A minimum requirement for analyzing resistivity logs is a knowledge of formation water resistivity. In examining the specific conductance[1] measurements of water samples from screened wells, it became apparent that conductance varied widely, both across the site and with depth. Hence an examination of the cause of these variations was carried out before examining the logs.

Specific conductance, pH, major ion concentrations, and concentrations of TCE and PCE, on water samples from screened wells were reported by WSRC (1990). The laboratory and field values of specific conductance (μS/cm) and pH were hand entered into a file and merged with a file of well locations and elevations of screened intervals obtained from Dennis Jackson of WSRC; a portion of the resulting file is shown as Table 2. Specific conductance and pH values measured in the field when the sample was obtained were entered into the file rather than the laboratory values; data were excluded if the laboratory and field values of fluid conductivity differed by more than 20%.

To examine the dependence of electrical conductivity upon water chemistry, we then chose a subset of data which would make the analysis manageable and would be representative of a wide range of natural and contaminated groundwaters. The subset used samples from the Lost Lake aquifer (mostly B and C screens) having cation and anion analyses. In other words, those samples in Table 2 having only pH, conductivity, TCE, and PCE analyses were dropped from the subset. Results from 57 samples selected from Table 2 are displayed in Figure 2. Two outstanding features can be noted in Figure 2:

1. The six samples with high pH ($11 < pH < 12$) and high conductivity (> 300 μS/cm) are characterized by low nitrate ($<$2ppm, except one sample), low TCE and PCE ($<$100ppm), sulfate in excess of 10ppm, and high sodium ($>$20 ppm).

2. The 51 samples with conductivity <300 μS/cm have pH values in the range 4.4-6.7 (with 2 exceptions). Nitrate values are less than 3 ppm for conductivity <50 μS/cm and then trend sharply upward as conductivity increases from 50 to 300 μS/cm (Figure 3).

These observations are explained in terms of the character of natural groundwater,

---

[1] Specific conductance, fluid conductivity, and fluid resistivity. Hydrologists and chemists report electrical conductivity of a fluid as specific conductance in units of μSiemens/cm. Geophysicists and petrophysicists report the same quantity as conductivity in units of Siemens/m (S/m) or as its reciprocal, resistivity in units of ohm-m. All refer to the same bulk electrical property of a material, in our case the electrical conductivity or resistivity of water. Suppose a sample has a specific conductance of 77 μS/cm. Then the conductivity is 77×10^{-6} S/cm = 77×10^{-6} S/10^{-2} m = 77×10^{-4} S/m. The resistivity, which is the reciprocal of conductivity, = $[77 \times 10^{-4}$ S/m$]^{-1}$ = 129.9 ohm-m. Thus a sample having a specific conductance of y in μS/cm has a resistivity of 10,000/y in ohm-m. In this report, specific conductance will refer to measurements in units of μS/cm whereas resistivity, designated by R, will refer to measurements in units of ohm-m.

contamination by cement leaching, and contamination by nitrate ion.

Character of natural groundwater. Natural, unpolluted groundwater in the A/M area is very fresh, as indicated by the large number of samples with Na and Cl concentrations of 1 to 2 ppm and conductivity between 20 and 40 μS/cm (500 to 250 ohm-m). As a consequence, only a small amount of solute is required to measurably increase the specific conductance.

Contamination by cement leaching. The highest conductivity samples (>300 μS/cm) are caused by leaching of the cement annulus in the wellbores, producing a high-pH electrolyte with enhanced sulfate and calcium. The association of high pH with leaching of cement in the wellbore is attributed to Van Price (Marine and Bledsoe, 1984, p. 7-5).

High sulfate seems associated with high pH. Michaus et al. (1989) describe the chemistry, manufacture, and setting reactions of portland cement; two aspects of their discussion are particularly germane to our observations: 1) After the mixture is heated in the kiln and before final pulverizing, a small amount of gypsum [$CaSO_4 \bullet H_2O$] is added to prevent premature stiffening of the cement when water is added. It does this by forming a trisulfoaluminate hydrate called ettringite which forms as needle-shaped crystals on the surfaces of tricalcium aluminate, thereby delaying hydration. 2) One of the hydration products is portlandite [$Ca(OH)_2$], which saturates the cement slurry's aqueous phase and raises its pH to between 12.5 and 13.0.

From these considerations, one expects that principal products from the leaching of cement in the wellbore annulus would be: calcium and hydroxyls from the portlandite in the aqueous/hydrous phase, and calcium and sulfate from ettringite which is disposed as a precipitate on grain surfaces. Thus, the handful of high conductivity samples having high pH and high levels of calcium and sulfate are compatible with what would be expected from leaching of cement. The locations of the high-pH samples are scattered throughout the A/M area (Figure 4), with a cluster of four in the north. Two of the eight high-pH samples have specific conductance values less than 100 μS/cm, the other six are all greater than 300 μS/cm.

Contamination by nitrate ion. Nitrate values are less than 3 ppm for conductivity <50 μS/cm and then trend sharply upward as conductivity increases from 50 to 300 μS/cm (Figure 3). Water conductivity values in the 50-300 μS/cm range correlate with an increase in nitrate and sodium concentration.

As there are no agricultural activities in the immediate area, the elevated nitrate levels are attributed to seepage of nitrate-rich (nitric acid waste) liquid from the settling basin into the groundwater: "Many of the processes in all three M-area facilities involve cleaning with caustic (sodium hydroxide) and hot nitric acid. These substances have been discharged to the process sewers. The nitric acid, even if neutralized, is a source of elevated nitrate discharges, some of which have migrated to the groundwater." (Marine and Bledsoe, 1984, p. 6-6)

Nitrate ion can be conserved in the near-surface. "In groundwater that is strongly oxidizing, NO_3^- is the stable form of dissolved nitrogen. It moves with the groundwater with no

transformation and little or no retardation. Very shallow groundwater in highly permeable sediment or fractured rock commonly contains considerable dissolved O_2. It is in these hydrogeolgic environments where NO_3^- commonly migrates large distances from input areas" (Freeze and Cherry, 1979, p. 413). Freeze and Cherry also state that a decline in the redox potential can in some situations cause NO_3^- to be reduced to N_2O or N_2. These products can exist as dissolved species and can be lost by outgassing to the atmosphere.

As a matter of interest, nitrate has been used as a tracer in drilling fluid by Chevron (Cooley, 1971), as a means of discriminating mud filtrate from formation water in samples. Fertilizer as source of nitrate was added to the drilling mud system. Fluid samples recovered from the well were then analyzed for nitrate, to determine whether the sample consisted of drilling mud filtrate (nitrate concentration equal to nitrate concentration in drilling mud), formation water (nitrate concentration near zero), or a mixture of filtrate and formation water (intermediate nitrate level).

Association between contaminant levels and specific conductance. Having discussed the three issues of the character of natural groundwater, contamination by cement leaching, and contamination by nitrate ion, we now discuss the empirical association of high conductivity and contaminant concentration.

When TCE (trichloroethylene) is plotted against PCE (tetrachloroethylene) concentration (Figure 5), a triangular pattern results. That is, for a given PCE concentration, TCE is as high or higher. This is of especial interest in light of Marine and Bledsoe's (1984, p. 6-6 and 7-2) comments that much larger quantities of PCE have been released than of TCE, and that PCE degrades anaerobically to TCE. Marine and Beldsoe (1984, Table 6-1) report 1,800,000 pounds of PCE and 317,000 pounds of TCE were released to the Settling Basin, whereas 1,000,000 pounds of PCE and 383,000 pounds of TCE were released to Tims Branch. Thus, 3 to 6 times as much PCE was released as was TCE. There are three possible reasons for the higher TCE concentrations in Figure 5: i) degradation of PCE to TCE, ii) the earlier release of TCE (1958 through 1970 to the Settling Basin) versus the later usage and release of PCE (1971 through 1979), and iii) higher solubility and higher mobility of TCE compared with PCE. In any case, we now follow the practice of Marine and Bledsoe (1984, p. 7-2), using the sum of TCE plus PCE as an overall indicator of contaminant concentration.

South and west of the settling basin, seven of eight samples with TCE+PCE in excess of 1000 μg/L also have conductivity values in excess of 100 μS/cm (Figure 6), and four of eight samples with TCE+PCE between 100 and 1000 μg/L have conductivity values in excess of 100 μS/cm. However, of the 12 samples with TCE+PCE less than 100 μg/L, only one has a conductivity value in excess of 100 μS/cm. Thus it appears that in this area, high water conductivity is associated with high values of TCE+PCE. It has already been noted that water samples with conductivity in excess of 100 μS/cm also have elevated concentrations of nitrate ion (5 to 25 ppm). Thus, as suggested by B. Looney (personal communication), it seems likely that nitrate and chlorinated hydrocarbon contaminants, which were co-released from the settling basin, have traveled along similar hydrologic pathways into and within the Lost Lake aquifer.

Elsewhere, and in particular to the north of the settling basin, there is no correlation between TCE+PCE concentration and conductivity.

Fluid conductivity distribution. The distribution of fluid conductivity is shown in vertical section in Figure 7 and as plan maps corresponding to four aquifer units in Figures 8-11. Water samples contaminated by contact with cement grout were excluded from the maps by dropping samples with pH greater than 8.0; however high pH samples are included in Figure 7 where pH is coded by symbol.

Ignoring the values with pH greater than 8, Figure 7 shows that conductivity ranges from 20 to 200 μS/cm in the upper hundred feet and ranges from 20 to 60 or 70 μS/cm in the elevation range 0 to 150 msl. In other words, a "knee" in the conductivity distribution appears in the middle of the Lost Lake Aquifer, above which conductivity values range higher than they do below the knee. Thus the data indicate a barrier to flow of nitrate-rich water near the middle of the Lost Lake Aquifer.

It is helpful to use Figure 7 as a reference while inspecting the maps of Figure 8-11. Starting from the bottom of the section, Figures 7 and 8 show that conductivity is low in all samples recovered from the Crouch Branch Aquifer. Conductivities remain low in the Crouch Branch Confining Zone (Figures 7 and 9), with the exceptions of an isolated high value northwest of building 321-M, and somewhat higher values north of the A-1 outfall. Within the Lost Lake Aquifer (Figures 7 and 10), conductivity is high west and south of the M-basin, remains low in the general area of building 321-M, and rises again north of the A-1 outfall. The fewer samples from the M-Area Aquifer (Figures 7 and 11) exhibit a spotty distribution; the highest values occur in the immediate vicinity of the M-basin.

In summary, the fluid conductivity distribution indicates that no nitrate-contaminated water has migrated downward into the Crouch Branch Aquifier, and that penetration into the Crouch Branch Confining Zone is very limited. Within the uppermost aquifers, high-conductivity water occurs most notably west and south of the M-basin. Figures 10 and 12 permit a comparison between the TCE+PCE and fluid conductivity distributions within the Lost Lake Aquifer. It appears that the association between high TCE+PCE and high conductivity (nitrate) occurs mainly to the west and south of the M-basin.

Table 2. Water analyses obtained in 1990 (Westinghouse Savannah River Co., 1990) from wells screened in the Lost Lake aquifer, ordered by conductivity. Field measurements are gallons extracted, conductivity (μS/cm), and pH. Laboratory analyses give cation and anion concentrations in mg/L; TCE and PCE in μg/L.

Well	-----Field-----			----Cations----			-----Anions----				
Name	Gal	Cond.	pH	Na	K	Ca	Cl	SO_4	NO_3/N	TCE	PCE
MSB-12A	240	19	4.7	1.3			1.8	1.0	0.3	624	4
MSB-41C	190	19	4.9							1	1
MSB-53B	190	19	5.3	1.7	0.5	0.7	2.1	1.0	0.5	1	1
MSB-43A	242	20	5.1	1.7			2.2	1.0	0.9	1	1
MSB-43A	240	20	4.5								
MSB-53C	102	20	5.2							1.8	1
MSB-13A	193	21	5.1	2.4	0.5	1.0	1.8	1.0	0.4	150	1
MSB-15AA	182	23	5.3	1.7	0.6	1.7	1.9	1.1	0.1	33	1
MSB-21B	200	23	5.5	1.6	0.5	1.7	1.5	1.0	0.7	272	2
MSB-43B	149	23	4.5								
MSB-43B	150	23	5.0	2.0			1.2	1.0	1.1	1	1
MSB-72B	124	23	5.2	2.4	0.6	0.7	1.8	1.6	0.3	1	1
MSB-21A	172	24	5.4	1.8			1.8	1.0	1.1	3	1
MSB-28A	182	24	4.9							3780	2
MSB-26A	138	25	5.0							108	17
MSB-42B	185	25	4.8							162	5
MSB-42C	96	25	5.2							18	2.5
MSB-55C	120	25	5.2	2.4	0.5	0.9	1.8	1.0	1.2	1	1
MSB-61C	138	26	5.2							1	1
MSB-68C	169	27	4.7	2.8	0.5	1.4	1.6	1.0	1.8	324	6
MSB-31B	154	28	4.9	2.1			2.0	1.0	1.3	316	26
MSB-34B	112	28	5.0							100	50
MSB-66C	162	28	6.1	3.4	0.5	1.7	1.2	1.0	1.2	62	13
MSB-29B	195	29	4.5								
MSB-16A	148	30	5.3							8315	126
MSB-37C	156	30	5.6							4	10
MSB-11B	171	31	5.7	1.6			1.8	1.0	0.2	176	2
MSB-44B	136	31	5.2							1	1
MSB-33B	221	33	5.1							17	26
MSB-11A	214	34	5.8	1.9			1.9	1.0	0.2	10	1
MSB-27B	158	35	5.2							122	1
MSB-30CC	166	35	5.1							1.1	1
MSB-29B	193	36	4.7	2.1			2.0	1.0	0.6	1	1
MSB-36C	80	37	5.1	2.4			1.9	1.0	1.9	210	18
MSB-45A	229	37	5.4							1119	248
MSB-20A	154	38	5.5	1.8			1.4	1.0	1.3	924	1
MSB-26B	221	38	5.7	2.1	0.5	3.1	1.9	1.0	0.5	268	2
MSB-45B	125	38	5.1							1	1
MSB-10B	154	39	5.0	2.5			2.1	1.0	0.1	30	73
MSB-29C	140	39	5.3	2.0			1.7	1.0	1.5	1	1
MSB-33C	110	39	5.1							19	11
MSB-73B	177	39	4.5	2.3	0.6	1.7	2.1	4.5	0.8	12	1
MSB-23B	134	40	5.1							532	13
MSB-15A	148	41	5.9	2.1			2.0	1.0	1.1	3310	112
MSB-18A	133	42	4.8	3.0			2.3	1.0	3.4	14	11
MSB-48C	125	42	5.8							105	1
MSB-50B	148	43	5.9							15	7
MSB-82C	143	46	6.1	4.5	0.7	30.0	2.0	1.0	1.3	1	1
MSB-09A	174	48	6.2	1.4			2.0	1.0	0.3	1880	2810
MSB-47C	104	51	5.5							7325	5
MSB-67C	151	51	5.8	3.1	0.7	3.9	1.9	1.0	1.9	65	1
MSB-19B	188	52	5.2	1.5			1.4	1.0	0.8	6	4
MSB-40B	156	53	5.1	1.7			1.8	1.9	1.0	685	1
MSB-46B	117	53	5.4							1	1

MSB-38B	190	56	6.4	4.4	1.4	5.2	1.7	1.1	1.4	899	598
MSB-49B	250	56	6.0							62	4
MSB-51B	138	58	6.0							1	1
MSB-35B	160	61	5.7							1	1
MSB-74B	174	61	6.3	5.1	1.2	4.4	1.7	2.2	1.0	2910	8
MSB-75B	136	61	5.6	13.0	1.4	6.2	1.7	6.5	2.7	461	1
MSB-84C	100	63	6.2							1	1
MSB-39C	70	64	4.8	3.7			2.1	1.0	3.2	64	11
MSB-11C	108	65	4.7	3.6			2.3	1.0	10.8	65200	72
MSB-30B	100	70	4.5							1	1
MSB-86C	164	70	6.4	12.0	0.5	1.6	1.5	5.5	1.2	1	1
MSB-31CC	94	74	6.2	2.4	0.8	7.2	1.4	1.5	2.7	288	11
MSB-38C	140	78	6.0	6.3	1.7	5.1	1.7	1.0	5.9	555	241
MSB-69C	26	79	6.3	5.0	1.8	6.5	2.3	1.2	2.9	84	1
MSB-52B	146	82	6.2							5	7
MSB-24A	6	86	4.5							34200	10900
MSB-83C	130	86	9.7	3.3	0.5	12.0	1.8	1.0	1.7	1	1
MSB-40C	40	87	5.5	1.8			2.0	9.1	0.4	4	1
MSB-76C	98	98	6.5							20800	170
MSB-54C	160	102	10.0							1	1
MSB-17BB	203	105	5.9	5.2	0.9	5.9	2.6	1.0	8.5	1735	430
MSB-75C	2	106	6.2	11.0	3.9	3.9	1.8	20.1	0.1	1	1
MSB-47B	174	110	6.2							1965	5
MSB-12B	154	132	4.4	15.0			3.6	1.0	12.3	7830	2600
MSB-64C	117	133	4.7	11.0	1.7	5.6	3.6	1.0	14.0	145	278
MSB-76C	98	142	6.7	24.0	0.9	1.5	2.2	16.2	2.0	19475	181
MSB-12C	130	152	4.9	15.0			3.9	1.0	14.6	2800	1140
MSB-70C	110	174	5.8	17.0	1.9	7.1	4.8	1.0	7.6	35	323
MSB-14A	183	186	4.6	9.6			3.8	1.0	13.2	1120	1650
MSB-17A	150	186	4.7	1.5			3.8	1.0	19.0	49	304
MSB-36B	160	221	4.9	1.4			2.8	1.0	23.5	1700	1
MSB-39B	190	242	4.7				4.4	1.0	20.4	198	210
MSB-79B	35	435	11.0	46.0	14.0	9.4	2.3	26.4	0.7	24	1
MSB-74C	16	473	11.2	23.0	20.0	15.0	1.2	16.3	0.1	13	1
MSB-85C	25	474	11.0							20	1
MSB-55HC	4	595	11.3	63.0	10.0	9.0	2.4	56.4	1.7	1	1
MSB-71B	43	1640	11.8	85.0	61.0	29.0	1.5	14.5	0.3	1	1
MSB-79C	3	2210	12.0	37.0	26.0	34.0	2.3	13.1	0.7	6	1
MSB-13B	2	2620	11.7	41.0	51.0	45.0	0.9	3.9	21.0	30	59

PHYSICAL PROPERTY DATA FROM CORE SAMPLES

Physical property measurements on core samples serve two purposes for log analysis. Parameters such as grain density are used directly in computing porosity from a density log. Parameters such as porosity and saturation determinations serve as checks on the results of log-based computations. Hence we examine here the results of previously published laboratory measurements.

Procedures. Samples collected from six MHB- and MHT- boreholes with a Shelby tube were analyzed by drying and weighing by Law Environmental of Atlanta, Georgia and the results reported by Eddy-Dilek and others (1993). The procedures, as explained by Michael O'Kelley of Law Environmental (personal communication) were as follows. Vertical samples up to 6 inches in length and 2.8 inches in diameter were extracted from the Shelby tube and trimmed to right circular cylinders. In addition, horizontal samples, typically 2 inches in length and 2 inches in diameter, were cut and measured. The volume V was computed from measured lengths, and a wet weight W_w was obtained. The sample was dried in an oven, and a dry weight W_d was obtained. Moisture content (percent) was computed as $MC(\%) = 100(W_w - W_d)/W_d$. Grain density ϱ_g was measured by pycnometer. The grain volume was computed as W_d/ϱ_g, and the porosity as $(V - W_d/\varrho_g)/V$.

Grain density. Grain density values are given in Table 3. Mean values of grain density decline somewhat, from 2.66 to 2.60, as sediment type progresses from "sandy fat clay" to "poorly graded sand", that is, as grain size increases. The mean grain density of 18 samples is 2.632 g/cm^3. Noting the limited range in measured grain density values, we used a fixed value of 2.63 g/cm^3 to calculate porosity from the density log.

Table 3. Grain density (specific gravity) values from Table 10 of Eddy-Dilek and others (1993), ordered by soil classification. Overall mean of 18 samples is 2.632.

Soil Classification	Grain Densities (g/cm^3)	Mean
Sandy fat clay	2.62, 2.72, 2.62, 2.66	2.660
Clayey sand	2.59, 2.67, 2.67, 2.65, 2.71	2.658
Silty sand	2.62, 2.65	2.635
Poorly graded sand with silt	2.59, 2.60, 2.53, 2.61, 2.62, 2.63	2.597
Poorly graded sand	2.62	2.620

Porosity. Excluding one high porosity (67%) sample, the mean porosity value for 17 vertically cut samples was 39.9% with a standard deviation of 2.70%. And excluding one high porosity (74%) sample, the mean porosity value for 11 horizontally cut samples was 38.0% with a standard deviation of 2.90%. Classifications included sandy fat clay, clayey sand, silty sand,

poorly graded sand with silt, and poorly graded sand. From these results, we can assume that 39% is a representative value for porosity for samples ranging from sandy clay to poorly graded sand recovered within 200 feet of surface, and that most samples (approximately two-thirds) will have values between 35% and 42%. Any bias in the measurement stems primarily from the effects of sample retrieval and handling. If a systematic bias exists, the porosity values are likely to be low, as sandy materials will be prone to consolidation during sampling and handling (M. O'Kelley, personal communciation).

Cation Exchange Capacity. Laboratory determinations of cation exchange capacity (CEC) on 18 samples are given in Table 4. Values of CEC decrease from a mean of 12.7 meq/100g in 4 sandy fat clay samples to a mean of 3.2 in six poorly graded silt-bearing sand samples. The electrical effect of clay in sandstones is expressed by the parameter Qv, which is the volume concentration of clay exchange cations in meq/ml. Qv measures the cation concentration in the pore space and is obtained from CEC by,

$$Qv = (CEC/100)\,\rho_g\,(1-\phi)/\phi \qquad (1)$$

Using our representative values of ρ_g=2.63 and ϕ=0.39, mean Qv values corresponding to mean CEC values were computed and entered in Table 4. By way of comparison, Waxman and Smits (1967) present Qv values for clean sandstones (porosity ~0.22) ranging from 0.02 to 0.08 and for very shaly sandstones (porosity ~0.28) ranging from 0.50 to 0.89. Thus, the values of Table 4 show that the A/M area samples lie in the middle of the Qv range bracketed by clean sandstones and shaly sandstones.

Table 4. Cation exchange capacity values from Table 19 of Eddy-Dilek and others (1993), ordered by soil classification. Qv is computed from CEC.

Soil Classification	Cation Exchange Capacity (meq/100g)	Mean CEC	Mean Qv
Sandy fat clay	8.6, 13.0, 8.0, 21.0	12.7	0.52
Clayey sand	4.6, 3.8, 6.4, 5.4, 7.2	5.5	0.23
Silty sand	4.5, 7.3	5.9	0.24
Poorly graded sand with silt	2.3, 3.3, 3.5, 3.2, 3.6, 3.3	3.2	0.13
Poorly graded sand	3.6	3.6	0.15

Water saturation. We are interested in obtaining estimates of water saturation from core samples to compare with estimates to be obtained from logs. Saturation was not reported, but can be computed from the moisture content data as $V_w/\phi = (MC(\%)/\phi(\%))\varrho_d$, where $\varrho_d = W_d/V$ is the dry bulk density (see preceding subsection "Procedures" for definition of variables). The result is given in column 3 of Table 5. Water retention data provide another measure of

expected saturation. The fourth and fifth columns of Table 5 are based on water retention by the wetting method. The mean values by wetting are quite comparable to the mean values by moisture content for the three intermediate soil classes, about 0.4. This agreement could be fortuitous. The moisture content measurements could be low due to moisture loss during sample handling. Water retention by wetting may be less applicable to our situation than water retention by drainage (Table 14, Eddy-Dilek and others, 1993), which gives higher values of residual saturation than do the data obtained by wetting. In any case, the values of water saturation displayed in Table 5 are probably a lower bound to the in-situ saturations in the vadose zone.

Table 5. Water saturation derived from moisture content, Tables 17 and 18 of Eddy-Dilek and others (1993). Water saturation by wetting at suction of 5 bars, Table 15. Samples ordered by soil classification. Asterisk* after mean value denotes exclusion of one sample from mean of the sandy fat clay class.

Soil Classification	Water sat. by moisture content.	Mean	Water saturation by wetting.	Mean
Sandy fat clay	0.51, 0.076, 0.46, 0.61	0.53*	0.91, 0.11, 0.62, 0.85,	0.79*
Clayey sand	0.29, 0.21, 0.40, 0.48, 0.43	0.36	0.31, 0.28, 0.56, 0.36, 0.54	0.41
Silty sand	0.31, 0.50	0.40	0.33, 0.41	0.37
Poorly graded sand with silt	0.22, 0.29, 0.27, 0.33, 0.48, 0.45	0.34	0.35, 0.27, 0.31, 0.44, 0.45, 0.36	0.36
Poorly graded sand	0.46	0.46	0.085	0.085

Clay Mineralogy. Inspection of 32 samples from the SRS, location and depth unknown, by DiStefano (1989) of Conoco, found kaolinite to be the dominant clay mineral, from 60 to 97% of a clay sample. Vermiculite (1 to 28%) and illite (<7%) were the two other clay minerals identified by DiStefano. These data and data from other investigators (Horton, 1995; U. of South Carolina, 1992) confirm that kaolinite is the dominant clay mineral. Horton (1995) also finds that illite was present in 21 of 22 samples, although in small amounts relative to kaolinite. Smectite was found to be present in 9 of 22 samples, and was the major clay component in 6 of these 9 samples.

Table 6. Chemical formula, grain density (g/cm^3), and thermal neutron response (equivalent water, volume percent of rock) of clay minerals found at Savannah River Site, from Ellis and others (1988). Cation exchange capacity (meq/100g) from Ruhovets and Fertl (1981).

Clay Mineral	Chemical Formula	ϱ_g	CEC	ϕ_{CNL}
Kaolinite	$Al_4(Si_4O_{10})(OH)_8$	2.64	3-15	45.1
Illite	$K_4(Al_8FeMg)(Si_{17}Al_3)O_{50}(OH)_6$	2.77	10-40	15.8
Vermiculite	$Mg_{.45}(Mg_{2.8}Al_{.2})(Si_{2.9}Al_{1.1})O_{10}(OH)_2$	2.54	--	8.8
Mont-morillonite	$Na(Al_5Mg)(Si_{12}O_{30})(OH)_6$	2.62	80-150	11.5

Electrical Resistivity - Previous Studies Experimental resistivity data on samples from SRS were purported to show that Archie's laws are not applicable at low saturations (Applied Research Associates, 1992). However, ARA's resistivity tests were done using deionized water with an initial (pre-test) resistivity of 1000 ohm-m. The expected resistivity values for the samples, calculated on the basis of Archie's laws, were much greater than those measured. The authors attribute this mismatch to a failure of Archie's laws. However, the usage of such an unrealistically high fluid resistivity produces flawed results because surface conduction becomes increasingly important at high fluid resistivity. The point at which this occurs depends upon clay content, but formation factor decreases below its nominal value as water resistivity exceeds 10 ohm-m, even in a clean sand (Hearst and Nelson, 1985, Figure 5-11). As discussed below in a section called "compensation for the effect of clay", we treat the problem by retaining the use of Archie's law and compensating for clay content by finding an apparent water resistivity which includes clay conduction effects.

LOG ACQUISITION AND PROCESSING

The hole locations for geophysical logs and penetrometer runs compiled as part of the present work are shown in three nested maps in Figures 13-15 and are tabulated in Appendix A. Penetrometer data are from the CPT-series of penetrations and geophysical logs are from the MSB-, MHT-, MHB-, and AMH- series of holes. Logs were obtained both in uncased (open) holes and in holes cased with 4-inch diameter PVC.

Open-hole geophysical logs. Graves Environmental and Geotechnical Services, Inc., Jackson, SC, performed most of the open-hole logging. Graves used logging tools manufactured by Century Geophysical of Tulsa, Oklahoma (Table 7). They typically acquired caliper, gamma ray, short (16-inch) normal resistivity, long (64-inch) normal resistivity, and SP logs (Figure 16). Graves Environmental does not have a license for nuclear sources, so when these were

requested for the MHT-holes, an affiliate, Graco Wireline Services, was called in from Tulsa. Graco also used Century tools, including a neutron, density, and resistivity guard log.

Logs were usually acquired by Graves shortly after cessation of drilling. Drilling typically progressed at 100 feet per day, so the 200-foot holes typical of the A/M area required two to three days to drill. Occassionally, a hole finished in the afternoon might not be logged until the next morning, but these occurrences were unusual. Water for the drilling mud came from one of two sources for the A/M area: a well at Building TC-1 or an outlet near the central shops; the drillers used Baroid Quik-Gel to make the drilling mud. No other additives were used, except perhaps for cottonseed hulls for controlling lost circulation.

Cased-hole geophysical logs. U.S. Geological Survey, Water Resources Division, Norcross, Georgia, acquired logs in MSB-holes after they had been cased with 4-inch diameter PVC casing. The USGS system used equipment manufactured by Comprobe, Inc (WSRC-RP-92-1302, pages 49 and C-8, Dec. 1992). Holes logged were: MSB-3B, MSB-3D, MSB-9A, MSB-10A, MSB-11A, MSB-15A, MSB-22, MSB-31A, MSB-43A.

Penetrometer logs. Applied Research Associates (ARA), Inc., South Royalton, Vermont, acquired cone penetrometer logs in holes prefaced with 'CPT' (Table A5 in Appendix A). The CPT logs discussed here have been displayed and described by Shinn and Bratton (1992) and by Looney and others (1992). For purposes of this report, we have retained six curves acquired by ARA, as listed in Table 8. Other curves (density, saturation, hydraulic conductivity) presented by Shinn and Bratton (1992) were derived using empirical relationships from one or more of the six curves listed in Table 7, and have not been retained in our data base. Figure 17 shows five curves from a typical penetrometer run, plotted in the same format as in Looney and others, 1992.

Well log data base. Data received from SRS personnel on diskettes were loaded into a commercial logging software package written by Terrascience, Inc. of Littleton, Colorado. Logs from Graves Environmental were digitized at a spacing of 0.1 feet, so this spacing was used for storing data in all boreholes. Logs from USGS-WRD, acquired at 0.2-foot spacing, were interpolated to 0.1 feet. Penetrometer data were acquired at a variable spacing of about 0.07 feet and were interpolated to 0.1 feet. Data are stored as "curves", by well. A curve can be an original log, core data, well construction data, or a computed log. Names of curves for logs and core data are given in Table 8. Well-by-well lists of logs, hole locations, date of logging, and types of ancillary well information are given in Appendix A.

Table 7. Logging tools and diameters (inches) manufactured by Century Geophysical Co. and measurement types. The second column gives the curve types recorded on floppy disk.

Tool	Measurements on disk	Comments
9040, 9041, 2.5"	gamma, fluid resistivity, SP, temperature, 16-inch normal, 64-inch normal	The 9041 has a lateral resistivity and a single point resistance, the 9040 does not.
9062 1.4"	caliper	
9060 1.4"	gamma, single-point, SP	Small diameter (1.5 inch) tool, hence gamma counts are lower than with other tools.
9030 2.2"	gamma, density (gamma-gamma), medium guard resistivity, caliper, porosity from density.	Because different grain density values were used, we did not enter the 'porosity-from-density'.
9055 1.8"	gamma, porosity-from-neutron, single point resistance, neutron counts (API), SP, slant angle, slant angle bearing, temperature	Because the porosity-from-neutron was computed incorrectly, we did not enter it. The slant angle bearing is corrected for magnetic azimuth if the magnetic declination is entered in the heading.
9071 2.9"	gamma, 16-inch normal, 64-inch normal, SP, Temperature, near and far thermal neutron detectors.	No data were acquired with the near and far neutron detectors.

Table 8. Definitions and units of curve names used in USGS logging data base.

PENETROMETER

Sleevest: Sleeve stress, in psi.
Tipstunc: Tip stress, uncorrected, in psi.
Tipstcor: Tip stress, corrected for pore pressure, in psi.
Ratiocor: Ratio of sleeve stress to corrected tip stress, in percent.
Porepres: Pore pressure, in psi.
Res: Resistivity from four-electrode array with one-inch spacing, ohm-m.

GEOPHYSICAL LOGS

Caliper: Borehole diameter, in inches.
Bit: Bit size, in inches.
Gamma: Natural gamma ray, in API units. Suffix of 30, 40, 55 denote 9030, 9040, 9055 tool models of Century Geophysical Co.
Density: Bulk density, in g/cm^3, from gamma-gamma detector.
SP: Spontaneous potential, in millivolts.
Res_16: Electrical resistivity, in ohm-m, from 16-inch normal array.
Res_64: Electrical resistivity, in ohm-m, from 64-inch normal array.
Res_pt: Electrical resistance, in ohms, from single electrode.
Res_mg: Electrical resistivity, in ohm-m, from medium guard array.
Res_fl: Fluid resistivity, in ohm-m, from a lateral device in a cage.
Temp: Temperature of borehole fluid, in degrees F.
Neu_api: Neutron-thermal neutron count rate, in API units.
Sang: Slant angle measured with inclinometers, degrees from vertical.
Sangb: Bearing of slant angle measured with magnetometers, degrees from north.

CORE DATA

Permv: Permeability of vertical plug, in cm/s.
Permh: Permeability of horizontal plug, in cm/s.
Porv: Porosity of vertical plug, in volume percent.
Porh: Porosity of horizontal plug, in volume percent.
Rhob: Bulk density, in g/cm^3.

GRAIN SIZE

Gravel: Gravel (>2mm) percentage from sieve analysis.
Sand: Sand (2mm - 0.0625mm) percentage from sieve analysis.
Clay: Clay (<0.0625mm) percentage from sieve analysis.
Modal: Most abundant grain size fraction, 1,...,12 : <0.0625,...,>256mm

WELL CONSTRUCTION

Grout: Depth interval (feet below surface) of grout emplacement.
Bentseal: Depth interval (feet below surface) of bentonite emplacement.
Sandpack: Depth interval (feet below surface) of sand pack.
Gravpack: Depth interval (feet below surface) of gravel.
Screen: Depth interval (feet below surface) of well screen.
Wtable: Depth interval (feet below surface) of water table.

Conversion of neutron logs

Neutron logs were acquired with Century's 9055 tool which uses a 1.0 Curie AmBe source separated by 14 inches (35.6 cm) from the center of a 1" x 6" Helium-3 detector. Tool response is specified as 0 to 10,000 API units to within ±5%. The API system is a single-point system: 1000 API units is assigned to the response of any neutron tool in a water-filled borehole of 7-7/8 inch diameter in Indiana Limestone of 19% porosity. The calibration hole is located at the API test pits in Houston. Each tool supplier develops a transform from API units to porosity for their own neutron tools.

The neutron porosity logs acquired in the MHT-series of boreholes were in error as received on disk. The count rate on disk matched the paper copies of the logs but the neutron porosity data did not and were obviously in error. Using calibration information supplied by Century Geophysical, we developed a conversion from countrate (in API units) to porosity:

$$y = \frac{a + c\ln x + e(\ln x)^2}{1 + b\ln x + d(\ln x)^2} \qquad (2)$$

where x is the count rate in API units, lnx is the natural logarithm of x, y is the porosity in percent, and the coefficients are given as a function of hole size in Table 9. At porosities less than 30%, the logarithm of count rate increases linearly with decreasing porosity, with uniform behavior as a function of hole size. However, at porosities greater than 30%, the curves for various hole sizes gradually converge to a single point at 100% saturation, requiring the complicated analytical form of equation 2. The form of the optimum fit and its coefficients were determined with commercial software called "Tablecurve". A spline algorithm interpolates to the correct hole diameter.

Table 9. Coefficients for converting from API counts to neutron porosity, Century Geophysical tool 9055. First column gives hole size in inches.

Dh	a	b	c	d	e
4	134.48	-.231455	-42.6678	0.00850	3.2358
6	141.95	-0.22097	-45.1699	0.006800	3.4608
8	155.469	-0.206884	-49.6559	0.0044381	3.846123
10	142.275	-0.212652	-45.6869	0.0056815	3.57950
12	62.9269	-0.27786	-20.5686	0.017538	1.6461

After conversion of porosity from percent to fractional units, the porosity is adjusted to a

sandstone matrix using $\phi_{ss} = 0.965\phi + 0.035$. This latter correction is required because the original transform was established for a limestone matrix. The correction was applied because the sediments at the Savannah River Site are sandy rather than calcareous. Final neutron porosity values are given as fractions rather than percent.

Correction of neutron tool in unsaturated rock.

Neutrons are moderated (slowed down) by hydrogen at low energies, and are also moderated by the rock matrix at high energies. Neutrons are not slowed down much in air. As a result, neutrons travel farther in partially saturated rock than in saturated rock. Consequently the neutron porosity reading is reduced, an effect which has been called the "excavation effect" by Segesman and Liu (1971) who present the corrections needed for compensated neutron logs from a Schlumberger tool. The corrections are maximum at 50% saturation and increase with increasing porosity. For example, a sandstone of 40% porosity and 50% saturation requires that 8.5% porosity be added to the log reading.

The question becomes, what is the 'excavation effect' for Century's single-detector thermal neutron tool? Fortuitously, the source-to-detector spacing for the near detector in Schlumberger's CNL tool is comparable to the 14-inch spacing of Century's single-detector tool. Ullo (1981), Figure 19, shows the correction for a 37% porosity clean sand for the near detector of Schlumberger's tool. Ullo shows a porosity correction of 3.3% at 50% saturation, so the correction is less than half that required for the Schlumberger compensated neutron tool. Following Segesman and Liu (1971) and using Ullo's (1981) result, an approximate correction algorithm for the Century neutron tool is,

$$\Delta\phi = 0.43\ (2\phi^2 S_w + 0.04\phi)\ (1\text{-}S_w) \qquad (3)$$

The correction $\Delta\phi$ should be added to the reading from a Century tool once the saturation S_w has been established.

Computation of porosity from density log.

In fully saturated rock, bulk density from the log ϱ_b, grain density ϱ_g, and porosity ϕ are related by,

$$\varrho_b = \varrho_g(1 - \phi) + \varrho_w\,\phi \qquad (4)$$

So that a density-derived porosity can be calculated as,

$$\phi_d = (\varrho_g - \varrho_b) / (\varrho_g - 1) \qquad (5)$$

In saturated rock, ϕ_d will equal the true porosity, but in unsaturated rock ϕ_d will be less than true porosity.

The SP response

An SP anomaly is established where a sand-clay interface is present, providing there is sufficient contrast between the resistivity of the borehole mud and the formation water. In MHT-7C, the larger SP anomalies are about 40 mV, typical of the MHT holes. The relationship between SP and resistivity at 70°F is,

$$SP(mV) = -71 \log(R_m/R_w) \qquad (6)$$

Accordingly, a 40 mV SP anomaly implies a contrast of 3.6 in R_m/R_w. In the MHT-holes, the SP voltage is low where the gamma ray log is high at a clay bed and is more positive where the gamma ray indicates the sand is relatively free of clay. That is, the SP log is reversed in character from the case in deep oilfield wells where saline formation waters cause $R_m > R_w$. For the 40-mV case in MHT-7C, we can state that R_m is about 1/3.6 or 0.27 the value of R_w. In other holes such as MHT-3C, the SP log variations remain reversed but are less than 10 mV, indicating that R_m and R_w are closer in value. We have not attempted to use the SP curves to estimate R_w, because the clay zones are generally so thin that a maximum excursion is difficult to pick, and because the SP curves are often of poor quality.

Filtering of nuclear logs

Overlays of gamma-ray logs in an MHT-hole showed that the fine structure was non-repeatable, and that filtering was required. Experimentation with several filters determined that an 11-point triangular filter preserved depth resolution and improved run-to-run repeatability. Because the log is digitized at 10 points per foot, the filter smooths over 1.1 feet of log. The curve labelled "gammaflt" contains the filtered gamma-ray log. The 11-point filter was also applied to density and neutron logs from the MHT-holes (Table 10).

Gamma-ray and density logs in cased holes

Gamma rays from the rock are attenuated by grout in the annulus between the PVC casing and the borehole wall. Taking the 11-inch bit diameter of MSB-3D as typical, then the annulus thickness is 3.5 inches. Gamma-ray attenuation through 3.5 inches of grout is expected to be around 50%. Potassium in grout, if present, could contribute to background activity. Figure 18 displays three gamma-ray logs from holes within 60 feet of one another. The correlative peaks, with less than three feet of vertical offset are evidence that gamma-ray logs are responding to the formation, despite the grout between the casing and formation. Trace-to-trace correlation diminishes below 100 feet. It appears that the gamma-ray logs from the cased holes can be used for correlation.

The density logs are a different story. Gamma rays from the source on the tool are precluded from sampling much of the formation because they are primarily scattered within the grout. Inspection of density logs in Looney and others (1992, Figures 3.3.3-3.3.11) shows the density logs are uncorrelated from hole-to-hole over short distances and also shows prominent

low-density "dropouts" which we attribute to the absence of grout. That is, the density log appears to be showing where grout voids occur within the annulus. Because the density tool is directional, these voids are not necessarily continuous around the hole.

Electrical resistivity normal logs.

The 16-inch and 64-inch resistivity measurements are specified over the 0 to 2000 ohm-m range; inspection of logs from MSB-holes shows maximum response to be at 3300 to 3400 ohm-m. The resolution of the single point resistance is no better than the 16-inch normal because the 8-inch hole size is too large for a point resistance tool. Because the 16-inch is on scale when the 64-inch is off scale and because its resolution is as good or better than the point resistance, the 16-inch reading is the more reliable of the three measurements.

Normal logs require correction for borehole fluid resistivity and hole size; the separation between the 16-inch and 64-inch logs in Figure 16 is caused by the high contrast between the mud resistivity and formation resistivity. Using a chart from Schlumberger, Scott (1978) wrote a Fortran code to correct the normal logs. The code requires the fluid resistivity, the hole diameter, and the tool diameter. This correction is applied to the logs before they are used quantitatively.

Corrections for guard resistivity log.

The Century 9030 density tool contains a guard resistivity sensor consisting of an 8-inch long center current electrode with constant-potential guard electrodes above and below it. Overall length of the three-electrode system is 55 inches; tool diameter is 2.2 inches. Its response range is 0 to 60,000 ohm-m to 5% accuracy. A correction chart furnished by Century shows that the measured resistivity must be multiplied by a factor which depends upon the ratio of measured resistivity to mud resistivity. For an 8-inch diameter hole, the factor ranges from 0.25 for $R_t/R_m=0.1$ to 1.46 for $R_t/R_m=1000$. The correction was applied by fitting polynomials to the Century chart and using the caliper measurement to interpolate between curves for varying hole sizes.

Compensation for the effect of clay.

To account for the presence of clay in sandstones, Waxman and Smits (1967) derived an empirical model which reduces to Archies law as the pore water becomes sufficiently conductive, but which accounts for a parallel conduction path due to clay counterions as the pore water becomes less conductive. However, the water resistivity in samples supporting the Waxman-Smits model is much less than the water resistivity at SRS (Figure 19). Consequently the empirical parameter in their model is not adequately constrained for high water resistivity. Our initial intention was to use the W-S model, incorporating the cation exchange capacity data described in a preceding section. However, the inadequacy of the model at high water resistivity made this impractical. Instead, we revert to the use of Archies law, as described in the next subsection. This appoach is tenable because water resistivity is derived from the log data, by

computing Rw in saturated sediments below the water table. An apparent Rw acquired in this fashion compensates for whatever effect clays have on water resistivity in the cleaner sands. In other words, we sidestep the issue of directly accounting for clay on electrical resistivity by making use of a direct in-situ measurement of effective water resistivity and then applying that measurement upwards into the vadose zone.

Computation of water resistivity, saturation, and bulk volume water.

Computation of water resistivity relies upon Archie's empirical law for a rock of porosity ϕ and resistivity R_o saturated with water of resistivity R_w, $R_o=R_w\phi^{-m}$. Rearranging this expression, we compute an apparent water resistivity curve $R_{wa} = R_{log}\phi^m$ where the empirical constant m=2. R_{log} is the guard resistivity or the 16-inch normal resistivity if the guard log is not available.

Saturation S_w is calculated by combining Archies expressions with the density log response. Archies' law relating the resistivity R_t of a partially saturated rock to its saturation is $R_t=R_oS_w^{-n}$. Combined with Archies' law for a saturated sample, $R_o=R_w\phi^{-m}$, we get

$$R_t = R_wS_w^{-n}\phi^{-m}. \qquad (7)$$

The density log in the unsaturated zone will read,

$$\varrho_b = \varrho_g(1 - \phi_v) + S_w\phi_v\varrho_w \qquad (8)$$

Solving eqn. 8 for ϕ_v and substituting into eqn. 7, assuming m=n=2, and solving for saturation S_w, we get,

$$S_w = \varrho_g / \chi\ , \qquad \chi = (\varrho_g - \varrho_b)(R_t/R_w)^{1/2} + \varrho_w \qquad (9)$$

In computing S_w, $\varrho_g = 2.63$ g/cm^3, ϱ_b is the density log, R_t is either the guard log or the 16-inch normal, and $\varrho_w = 1.0$ g/cm^3 for fresh water. R_w is obtained by averaging the water resistivity curve R_{wa} defined above, within the sandy zones below the water table. By this procedure, R_w includes the excess conduction provided by clay minerals.

The solution of eqn. 8 for porosity in the vadose zone is

$$\phi_v = (\varrho_g - \varrho_b) / (\varrho_g - S_w\varrho_w) \qquad (10)$$

where S_w has been set to 1.0 wherever it exceeds 1.0 as a result of low values of R_t in eqn. 9.

Finally, water content, here called bulk volume water, (fraction of volume pore water per rock volume), is computed in the vadose zone as the product,

$$Bvw = S_w\phi_v \qquad (11)$$

Table 10 and Figure 20 summarize the computational procedures. Table 10 lists the equivalence between curve names and mathematical symbols. For example, porosity curve Vadpor is equivalent to ϕ_v.

Table 10. Computed curves based upon geophysical logs, arranged in approximate order of computation. Refer to Table 8 for definitions of original curves.

Curve Name	Computation	Curve Inputs and Constants
Densityf	Densityf = Density⊗[1,2,3,4,5,7,5,4,3,2,1]	
Denporf	$\phi_d = (\varrho_g - \varrho_b) / (\varrho_g - 1)$	$\varrho_g = 2.63$, ϱ_b = Densityf
Gammaflt	Gammaflt = Gamma⊗[1,2,3,4,5,7,5,4,3,2,1]	
Neupor	Neupor = f(Neu_api, Caliper)	Caliper = Cal30
Neuporf	Neuporf = Neupor⊗[1,2,3,4,5,7,5,4,3,2,1]	
Neuporfc	$\phi_c = \phi + 0.43(2\phi^2 S_w + 0.04\phi)(1-S_w)$	ϕ = Neuporf, S_w = Sw
Res_16rm	Res_16rm = f(R_m, Dh, Dt, Res_16)	R_m = avg(Res_fl) Dh = Cal30, Dt = 2.5 inches
Res_64rm	Res_64rm = f(R_m, Dh, Dt, Res_64)	R_m = avg(Res_fl) Dh = Cal30, Dt = 2.5
Res_mgc	Res_mgc = f(Res_mg, Dh, Rm)	R_m = avg(Res_fl) Dh = Cal30
Rwa	$R_{wa} = R_{log}\phi^2$	R_{log} = Res_mg or Res_16rm, ϕ = Denporf
Sw	$S_w = \varrho_g / \chi$, $\chi = (\varrho_g - \varrho_b)(R_t/R_w)^{1/2} + \varrho_w$	$\varrho_g = 2.63$, $\varrho_w = 1.0$ ϱ_b = Densityf, R_t = Res_mg or Res_16rm, R_w = avg(R_{wa}),
Swlim	$S_{wlim} = S_w$ $(S_w < 1)$ $S_{wlim} = 1.0$ $(S_w > 1)$	S_w = Sw
Vadpor	$\phi_v = (\varrho_g - \varrho_b) / (\varrho_g - S_w\varrho_w)$	$\varrho_g = 2.63$, ϱ_b = Densityf, S_w = Swlim, $\varrho_w = 1.0$
Bvw	$Bvw = S_w\phi_v$	S_w = Swlim, ϕ_v = Vadpor
Clayflag	Clayflag = 1.0 where R < Rlimit or $\phi_c > \phi$limit.	R = Res_mg or Res_16rm, Rlimit ≈ 400 ϕ_c = Neuporfc ϕlimit = 0.55

DISCUSSION

Overview. Well MHT-9C (Figure 21) was chosen as an example for discussion because it has a complete suite of logs all of which are on scale from surface to total depth. The two right-hand columns contain a summary of the computational results, specifically as the Sw, Clayflag, Bvw, and Vadpor curves. These four curves suggest a three-way partition of the lithologies in the vadose zone into clay-rich, high-silt/low-clay, and partially saturated sand zones. Clay-rich zones occur where the Clayflag is turned on in response to low resistivity or high neutron porosity. High-silt/low-clay zones occur where Clayflag is off and where the rock is saturated or nearly so (absence of waffle grid). Partially saturated sand occurs where saturation Sw is less than 1, that is, where the waffle grid denotes that moisture content, Bvw, is less than vadose-zone porosity, Vadpor.

It should be emphasized that the three-way partition relates to pore space properties which are related to lithological and mineralogical properties. Water saturation is related to specific surface area, which in turn is related to grain size and packing. Water saturation is expected to be high in beds with a high fraction of clay-size particles and low in beds comprised of clean, well-sorted sand.

This three-way division of the vadose zone is important in terms of contaminant, water, and gas transport. Clay-rich zones are likely to be much less permeable to all three fluids, are likely to "pond" downward-moving dnapl, and are known to contain dnapl contaminant (J. Rossabi, pers. comm.). High-silt/low-clay zones are likely to block air flow, offer low relative permeability to water and contaminants, and are likely to trap residual contaminant. Partially saturated sands provide the highest relative permeability to water, gas, and contaminant, but are not likely to trap residual contaminant.

We now discuss some specific features of the logs which support this three-way division, and also some of the problem areas which limit the reliability of the results.

Porosity. Porosity is remarkably constant throughout the section penetrated by MHT-9C. Excluding the clay-rich zone from 85 to 112 feet, the log-computed porosity, Vadpor, ranges from 0.34 to 0.55 with a mean of 0.437. Porosity in the saturated zone, 148 to 182 feet, is 0.45, only slightly greater than porosity in the unsaturated zone, 0.43. The log-derived mean of 0.44 is 0.05 higher than the mean porosity of 0.39 obtained from Shelby tube samples, as described in the section on physical property data. The discrepancy of 0.05 could be caused by a grain density value being too high, a density log reading too low, or inadvertent packing of the Shelby tube samples. In any case, both the logs and the core samples show that porosity is remarkably constant within the section.

Indicators of partial saturation. Partial saturation affects both original and computed logs in recognizable ways, as can be observed in Figures 21-24. Because grain density and porosity do not vary much in these holes, bulk density (in column 1) decreases where saturation decreases. However, bulk density also decreases where clay content is high, so a better indicator is the

separation between the two porosity curves derived from the density and neutron logs, denporf and neuporfc (column 4 of Figure 24, 40-90 feet). In zones of partial saturation, the neutron porosity decreases because there is less hydrogen in the rock. However the density porosity, denporf, increases because the density log decreased due to air-filled pore space. Note that vadpor, the porosity estimate which has been compensated for saturation, does not change in the partially saturated zone. The separation between neutron and density logs is commonly used in oil wells to find gas zones.

Another indicator of partial saturation is the apparent water resistivity curve, Rwa, in column 3 of Figure 24. Rwa values are high in partially saturated zones, tracking the guard resistivity although it is compensated for porosity fluctuations.

Saturation Sw anticorrelates crudely with modal grain size, in column 5, Figures 21-24, and also with sand and gravel fraction, that is, with 100 - clay in column 2. Both modal grain size and sand+gravel increase as surface area decreases. Surface area is the actual control on Sw.

These qualitative indicators concur with the changes in saturation shown by the waffle grid in column 6. The waffle grid shades the area between vadpor = ϕ_v, from eqn. 10, and Bvw = $S_w\phi_v$, from eqn. 11. Thus the waffle grid shows the volume fraction of air in rock, $\phi_v(1 - S_w)$. The wavy shading shows Bvw, the volume fraction of water in rock.

Gamma-ray log, grain size data, and the tan clay. Although the gamma-ray log correlates fairly well with clay-size fraction (column 2 of Figures 21-24), exceptions show that it is not a reliable predictor of the clay-size fraction. The most notable exception is the "tan clay" interval (99-110 feet in MHT-9C, 101-113 feet in MHT-3C, 102-115 feet in MHT-7C) which is characterized by low resistivity and high clay-size fraction from sieve analysis. The gamma-ray log increases at the tan clay in MHT-7C, in the other two holes it does not. In MHT-7C, the neutron porosity increases, but it remains relatively unchanged in MHT-9C. The mix of log responses in the tan clay in three different holes suggests that clay minerals and associated mineral phases vary from hole to hole. Horton (1995) notes that two xrd samples from the tan clay, from wells MSB-3B and MSB-79C, indicate smectite, kaolinite, and minor illite. Using the physical properties of clays (Table 6) to interpret the log responses, we can make some qualitative assertions about clay composition within the tan clay. For example, all logs respond in MHT-7C, so it is likely that illite (potassium emits gamma rays), smectite (high CEC causes low resistivity), and kaolinite (high water content increases neutron porosity) are all present in significant quantities. Hole MHT-9C, with no gamma response but with pronounced resistivity and neutron responses, is likely to contain smectite and kaolinite, with little illite and heavy minerals. The subdued responses in MHT-3C suggests that total clay content is less than in MHT-7C or MHT-9C. We caution that these associations are speculative and point out the need for coordinated work in clay mineralogy and log analysis.

Lithology and clay mineralogy in MHT-1C. Rine (U. South Carolina, 1992, p. 8) describes the core from MHT-1C. To demonstrate that the logs are compatible with core description, we compare this description (italics) with the logs of MHT-1C in Figure 22. *The Upland unit in*

MHT-1C (0-47') consists generally of coarse-grained sand with abundant pebbles and interstitial clay. A thick bedded clay is present at the top (5'-14') and at the base of the unit (37'-42'). The upper interval is only partially logged, but the lower clay unit is shown as a low-resistivity, high-neutron, high-gamma unit which produced a computation of full saturation and triggered the clay flag.

The Tobacco Road Sand (47'-153') consists of fairly clean sand with lenses of pebble rich sand mud layers. The top of this unit (49'-61') is especially striking ... this medium-grained, moderate- to well-sorted interval ... has a fining-upward trend similar in character to sequences found in fluvial meander belt systems. The resistivity and gamma-ray logs indicate a fining-upward trend from 65' to 49'.

Clay mineralogy in MHT-1C is described by Segall (U. South Carolina, 1992, p. 29). *Samples from 7' to 69.5' depths contain well-crystallized authigenic kaolinite... Below 170' depth the sediments contain 26-58% relative abundance of smectite and fecal pellets, indicating they may belong to the Dry Branch Formation.* The observation of smectite is important, because the decreasing resistivity from 170 to 185 feet could be due to increasing smectite abundance. Horton (1995) also finds smectite in four samples from a depth range of 145 to 167 feet.

Effect of bed thickness and invasion on resistivity logs. Inspection of Figure 25 shows that bed resolution increases progressively from the normal to the guard to the penetrometer logs. For example, a low resistivity bed at 129 feet in MHT-9C is shown by the guard resistivity to be about 2.5 feet thick. The 16-inch normal log defines the thickness adequately, although the bed resistivity response is not as low as the guard resistivity. The 64-inch resistivity shows a bed thickness of about five feet, which is an artifact of the 64-inch spacing rather than the true bed thickness. Note that the 64-inch resistivity reading is not as low as either the guard or 16-inch readings. This example simply illustrates that the 64-inch tool, designed for deeper penetration, is not as effective at either defining bed thickness or measuring bed resistivity as either the 16-inch tool or the guard tool.

Now compare the character of the resistivity curve from the penetrometer run in CPT-007a with that of the resistivity logs from hole MHT-9C (Figure 25). The bed resolution is of course much better than the three geophysical logs because the penetrometer electrode spacing is one inch. There is no effect from mud that requires compensation. And there is no invasion of filtrate into the formation. The only flaw of the penetrometer resistivity is the nearly flat resistivity of 7000 to 8000 ohm-m recorded from 50 to 85 feet. Other than this apparent measurement limitation at very high resistivities, the penetrometer does an excellent job of measuring formation resistivity and resolving thin beds.

When holes are drilled, mud filtrate invades the sand units while a mud cake forms. As a result, the sand units contain an amount of fluid of lower resistivity than the formation water, reducing the resistivity reading. The depth of invasion is probably not great because of the relatively high porosity. However, no attempt has been made thus far to assess the effect of

invasion upon the normal and guard logs.

Resistivity patterns from penetrometer runs. Resistivity logs from 15 penetrometer runs (Figure 26) are grouped by their location with respect to the settling basin. Refer to the map of Figure 13 for CPT locations. The resistivity values below depths of 130 feet, the approximate depth of water table, are less for the penetrations south of the settling basin than for those west or north of the basin. In particular, mean values at 145 feet in the southern runs are roughly 1/3 of the mean values of the western runs. These lower resistivity values could be indicative of lower water resistivity associated with elevated nitrate concentrations, as discussed previously under "groundwater chemistry". It is tempting to compare the resistivity patterns of Figure 26 with the fluid conductivity patterns in the Lost Lake and M-Area aquifers (Figures 10 and 11). With two exceptions, the two patterns appear compatible, although one must remember that the fluid conductivity values date from 1990 while the penetrometer runs date from 1992. Spreading of a nitrate plume during the two-year hiatus would produce a broader resistivity pattern than the one indicated by the fluid conductivity map.

However, there is also the possibility that the reduced resistivity values reflect more smectite in the southern holes than elsewhere. The high CEC of smectite (montmorillonite, Table 6) means that resistivity is more sensitive to smectite concentration than to other clays. Before the resistivity patterns can be used to track a nitrate plume, the smectite concentration and distribution needs to be better understood.

Sensitivity analysis. How good are the calculated logs of saturation and porosity? To determine their sensitivity to systematic measurement errors, eqns. 9-11 were coded in Fortran, and a base case was selected from a depth of 55.5 feet in MHT-9C. The four input base case parameters were Rhog = ϱ_g = 2.63 g/cm^3, Rhob = ϱ_b = 1.75 g/cm^3, R_t = 1400 ohm-m, and R_w = 165 ohm-m. Output values were S_w = 0.738, Vadpor = ϕ_v = 0.465, and Bvw = 0.343. Agreement between the base case values computed with the log processing software and with the Fortran code for sensitivity analysis provided a quality check on the two respective codes.

Ranges of values were chosen for the four input parameters which were deemed to be reasonable in terms of measurement reliability. The range for ϱ_g was chosen as $\pm$0.04 g/cm^3, which spans the range of mean values of the five sample classes in Table 3. The range for ϱ_b was chosen to be $\pm$0.05 g/cm^3, which is a conservative range for the accuracy of a density log. The accuracy for R_t and R_w was estimated at $\pm$20%, which greatly exceeds the tool specifications.

Results of the sensitivity analysis are shown in Figure 27, in the form of a 3x4 plot matrix, with the three outputs shown in successive columns. Of the four input parameters, errors in grain density (or variations of grain density with depth) have the least impact on output parameters. The effect upon S_w and ϕ_v is equal and opposite for errors in both ϱ_g and ϱ_b, so that Bvw is completely insensitive to systematic errors in either ϱ_g or ϱ_b. Uncertainty in either R_t or R_w produces significant error in both S_w and Bvw. However, if the values of both R_t or R_w are less than true values, as is likely to be the case in clean resistive sands, then their effects

tend to cancel. For the ranges of values chosen, the resulting error in ϕ_v is only 0.02 to 0.03, which is quite tolerable.

RECOMMENDATIONS

Our recommendations fall into three categories: improvement of present logging procedures, analysis of existing logs, and geological correlation.

The utility of geophysical logs would be greatly enhanced by upgrading to a more complete suite of logging measurements. The improvements are illustrated by the contrast between the logs acquired in the MHT-holes (Figures 21-24), as contrasted with those routinely acquired (Figure 16). The guard resistivity log is demonstrably superior to the normal resistivity log: bed definition is better, dynamic range is greater, and it requires less correction for borehole effects. Although we have not illustrated the dynamic range problem in this report, both the guard tool and the 64-inch normal tool are inadequate at high resistivity, often producing a straight-line log in the sandy sections of the vadose zone. A remedy to this problem will require collaboration with the tool manufacturer. A density log is needed for accurate porosity determination. A neutron log is very helpful in determining high clay zones, especially so at SRS because the gamma-ray log does not respond to the high kaolinite zones.

Analysis of existing logs must emphasize the electrical resistivity logs, which along with the gamma ray logs were collected in all holes. The penetrometer logs have excellent resolution and can be used directly, their only limitation is loss of fidelity in the high resistivity zones. The guard resistivity logs require a straightforward correction; bed definition is quite good. However, the existing 16-inch and 64-inch normal resistivity logs require careful treatment. We recommend that they be interpreted quantitatively using inversion techniques which derive the bed thickness and bed resistivity directly from the uncorrected logs (Whitman, 1995; Whitman and others, 1989). The inversion procedure would provide estimates of R_t more accurately than is possible by the method described in this report. Improved estimates of R_t would greatly improve the computed S_w logs. Improved bed definition, a result of the inversion, would greatly improve the delineation of high-clay beds and the correlation between holes.

At this point it becomes difficult to separate the goals of log analysis and correlation work. Some specific targets are delineation of the high-clay zones and determining whether or not a nitrate plume can be traced with electrical resistivity logs. Reduced resistivity values from the cone penetrometer runs south of the settling basin may be indicative of a nitrate plume, but the competing influence of smectite must be examined. If smectite turns out not to be a significant contributor or if its effects can be sorted out, then logging of existing cased holes with an induction tool could be useful in tracking a conductive plume.

Correlation work within the A/M area will use the four logging data sets discussed in this report: 1) the high resolution stress and resistivity logs from the cone penetrometer, 2) the complete suite of geophysical logs from the MHT-holes, 3) the gamma ray and normal resistivity

logs available from open holes, after inverting to bed properties, and 4) the gamma ray log from the cased holes.

Correlation work should be undertaken by a combined team of a log analyst, a stratigrapher, and a clay mineralogist. Correlation of the geophysical and penetrometer logs alone would serve to link zones of equivalent physical properties, but these need to be interpreted within the context of fluvial/deltaic geology. High-clay zones and fine-grained units need to be interpreted in terms of contaminant retention. By coordinating these disciplines, a much improved definition of flow paths and zones of contaminant retention can be achieved. Improved definition of retention will aid in assessing contaminant location and inventory in rock.

ACKNOWLEDGEMENTS

Ed Rooks of Graves Environmental and Geotechnical Services, Inc., Jackson, South Carolina, supplied information regarding drilling and logging procedures. Brian Peterson of Century Geophysical, Tulsa, Oklahoma, provided information regarding Century's logging tools.

REFERENCES

Cooley, B.B., 1971, Nitrate in drilling fluid as a tracer ion, Trans. 12th Annual SPWLA Logging Symposium, p. D1-D7.

DiStefano, M.P., 1989, Characterization at the Savannah River Plant: Mineralogy, Conoco Technical Service Report No. 1809-005-01101-89, 10 p.

Eddy-Dilek, C.A., Looney, B.B., Hazen, T.C,, Nichols, R.L., Fliermans, C.B., Parker, W.H., Dougherty, J.M., Kaback, D.S., and Simmons, J.L., 1993, Post-test evaluation of the geology, geochemistry, microbiology, and hydrology of the in situ air stripping demonstration site at the Savannah River Site, Westinghouse Savannah River Company, Report WSRC-TR-93-369 (Rev 0), 76 p.

Ellefsen, K., 1995, High resolution mapping of stratigraphy using seismic tomography: a feasibility test at the M-area basin, Savannah River Site, South Carolina, USGS Open-file Report, 44 p.

Ellis, D., Howard, J., Flaum, C., McKeon, D. Scott, H., Serra, O., and Simmons, G., 1988, Mineral logging parameters: nuclear and acoustic, The Technical Review, v. 36, n. 1, p. 38-52.

Freeze, R.A., and Cherry, J.A., 1979, Groundwater, Prentice-Hall, Inc., 603 p.

Hearst, J.R, and Nelson, P.H., 1985, Well logging for physical properties, McGraw-Hill Book Co.

Horton, R., 1995, X-ray diffraction studies of selected core samples from A/M area, Savannah River Site, South Carolina, USGS Open-file Report, 26p.

Looney, B.B., Rossabi, J., Tuck, D.M., Jordan, J.E., Bergren, C.L., Stevenson, A.E., Kristiansen, B.S., 1992, Assessing DNAPL contamination in A/M Area, SRS: Phase I results (U), Westinghouse Savannah River Company, WSRC-RP-92-1302, 91 p.

Marine, I.W., and Bledsoe, H.W., 1984, Supplemental techical data summary, M-Area groundwater investigation, DPSTD-84-112, E.I. duPont de Nemours & Co., 253 p.

Michaus, M., Nelson, E., and Vidick, B., 1989, Cement chemistry and additives, Oilfield Review, v. 1, n. 1, p. 18-25.

Robertson, P.K., and Campanella, R.G., 1989, Guidelines for geotechnical design using the cone penetrometer test and CPT with pore pressure measurement, Hogentogler & Company, Inc., Columbia, Md., 194 p.

Ruhovets, N., and Fertl, W.H., 1981, Digital shaly sand analysis based on Waxman-Smits

model and log-derived clay typing, paper V in Transactions Paris Symposium, Soc. Prof. Well Log Analysts, pp. 107-134.

Segesman, F., and Liu, O., 1971, The excavation effect, paper N in Transactions of Twelfth Annual Logging Symposium of Society of Professional Well Log Analysts, 24 p.

Scott, J.H., 1978, A Fortran algorithm for correcting normal resistivity logs for borehole diameter and resitivity, USGS Open-File Report 78-669, 12 p.

Shinn, J.D., and Bratton, W.L., 1992, Piezo-resistivity electric cone penetration technology investigation of the M-basin at the Savannah River Site, Aiken, South Carolina, Applied Research Associates, Inc., South Royalton, Vermont, 180 p.

Ullo, J.J., 1981, Response of the dual spacing neutron log (CNL) to gas, SPE Paper 10295, 56th Annual Technical Conference of Society of Petroleum Engineers, 11 p.

U. South Carolina, 1992, Sedimentology and stratigraphy of the Upland Unit, SCUREF Cooperative Agreement, Task Order No. 53, Progress Report, Dec. 2.

Waxman, M.H., and Smits, L.J.M., 1968, Electrical conductivities in oil-bearing shaly sands, Soc. Petroleum Engineers Journal, Transactions AIME, v. 243, p. 107-122.

Westinghouse Savannah River Company, 1990, The Savannah River Site's groundwater monitoring program, Third Quarter 1990, ESHEMS-900133 p. 526-609.

Westinghouse Savannah River Technology Center, 1993, Microscopic examination of sediment cores, Manual WSRC-L14.1, Procedure 2-15, Rev.2, 11 p.

Whitman, W.W., 1995, Interpretation of unfocused resistivity logs, The Log Analyst, v. 36, n. 1, p. 35-39.

Whitman, W.W., Towle, G.H., and Kim, J.H., 1989, Inversion of normal and lateral well logs with borehole compensation, The Log Analyst, v. 31, n. 1, p. 10-19.

APPENDIX A. LOGS, HOLE LOCATIONS, AND OTHER CURVES IN DATA BASE FOR A/M AREA

The five tables of Appendix A give the hole name, hole location, types of logs, types of other curves, and date of logging, where available. These data are entered into the USGS data base established for this project, based upon diskettes furnished to the authors by WSRC personnel. The data are stored at a spatial scale of 10 per foot, under software written by Terrascience, Inc. of Littleton Colorado.

Table A1. Geophysical logs and other curves in MSB-series of holes. Logs supplied by Graves in open holes where resistivity logs are listed, otherwise logged by USGS in cased holes.

MSB wells	East	North	Logs	Other Traces	Date
01B	48483.2	101833.0	caliper, gamma, sp, res_16, res_64,rm, rm_temp	bit	8/2/90
02B	48748.2	101997.9	caliper, gamma, sp, res_16, res_64, rm, rm_temp	bit	8/21/90
03B	48568.0	102191.7	caliper, density, gammaray, amplitud, rm, rm_temp	gravel, sand, clay, grout, bentball, sandpack, gravpack, screen	GRAVES 9/5/90 USGS 3/30/92
03D	48524.6	102188.6	caliper, density, gammaray	grout, bentball, sandpack, gravpack, screen	
04B	48312.8	101978.3	gamma, sp, res_16, res_64, res_pt, rm, rm_temp	bit	8/9/90
09A	48242.5	102236.7	caliper, density, gammaray		3/30/92
10A	47954.4	102451.8	caliper, density, gammaray		
11A	48577.6	102638.9	caliper, density, gammaray		
15A	48827.0	102983.5	caliper, density, gammaray		
15B	48818.5	102953.2	caliper, gamma, sp, res_16, res_64	bit	2/15/89
17BB	46220.8	102009.5	gamma, sp, res_16, res_64, res_pt		12/14/88
22-	48508.8	102186.5	caliper, density, gammaray	grout, bentball, sandpack, gravpack, screen	
23TAR	49225.8	104298.8	caliper, gamma, sp, res_16, res_64, res_pt	bit	6/4/93
26AA	48941.7	104612.8	gamma, sp, res_16, res_64, res_pt		2/6/89
31A	50100.2	101979.3	caliper, density, gammaray		3/30/92
31BB	50067.9	101983.1	caliper, gamma, sp, res_16, res_64, res_pt	bit	2/16/89
43A	49293.7	107275.3	caliper, density, gammaray		

48C	54077.0	107917.5	caliper, gamma, sp, res_16, res_64, res_pt	bit	5/23/89
49A	45864.6	99759.0	caliper, gamma, sp, res_16, res_64, res_pt	bit	1/13/89
53B	54574.3	106443.6	gamma, sp, res_16, res_64, res_pt	bit	2/1/89
55C	52029.7	108324.6	caliper, gamma, sp, res_16, res_64, res_pt	bit	4/26/89
61C	55406.6	106091.1			3/20/81
62B	47906.8	101865.3	gamma, sp, res_16, res_64, res_pt, rm, rm_temp	bit	11/5/90
66TA	51096.7	105842.6	caliper, gamma, sp, res_16, res_64	bit	9/7/88
67B	51989.6	106842.0	caliper, res_16, res_64, res_pt	bit	10/19/88
68B	52308.5	106744.9	caliper, gamma, sp, res_16, res_64, res_pt	bit	11/17/88
69TA	52418.4	107772.5	caliper, gamma, sp, res_16, res_64, res_pt	bit	12/22/88
71B	44054.7	103801.6	caliper, gamma, sp, res_16, res_64, res_pt	bit	10/10/88
72B	48350.3	96387.6	gamma, sp, res_16, res_64, res_pt	bit	1/24/89
73B	45694.0	99270.3	gamma, sp, res_16, res_64, res_pt	bit	2/2/89
75B	48875.5	98937.4	gamma, sp, res_16, res_64, res_pt, rm, rm_temp	bit	10/27/89
82C	51949.4	107521.9	gamma, sp, res_16, res_64		5/11/89
83C	52384.7	108405.3	caliper, gamma, sp, res_16, res_64, res_pt	bit	5/8/89
84C	51973.7	108967.9	caliper, gamma, sp, res_16, res_64, res_pt	bit	5/2/89
85C	53151.4	107835.2	gamma, sp, res_16, res_64, res_pt	bit	5/17/89

Table A2. Geophysical logs and other curves from MHT-series of holes. Logged by Graves, Jackson, SC or Grayco, Tulsa OK.					
MHT wells	East	North	Logs	Other Traces	Date
01c	48765.6	102706.8	gamma40, sp, res_16, res_64, res_pt, temp, res_fl, gamma30, density, res_mg, cal30, gamma55, neu_api, sang, sangb	bit	1/24/90
02c	48780.3	102747.1	gamma40, sp, res_16, res_64, res_pt, temp, gamma30, density, res_mg, cal30, gamma55, neu_api	bit	2/8/90
03c	48861.1	102704.3	gamma40, sp, res_16, res_64, res_pt, temp, res_fl, gamma30, density, res_mg, cal30, gamma55, neu_api, sang, sangb	bit, cec, toc, gravel,sand, clay, modal	1/25/90
04c	48863.5	102778.9	gamma40, sp, res_16, res_64, res_pt, gamma30, density, res_mg, cal30, gamma55, neu_api	bit	2/9/90
05c	48905.9	102725.1	gamma40, sp, res_16, res_64, res_pt, gamma30, density, res_mg, cal30, gamma55, neu_api, sang, sangb	bit, cec, toc, gravel,sand, clay, modal	1/29/90
06c	48900.0	102810.8	gamma40, sp, res_16, res_64, temp, res_fl	bit	3/2/90
07c	48977.5	102788.9	gamma40, sp, res_16, res_64, res_pt, res_fl, gamma30, density, res_mg, cal30, gamma55, neu_api, sang, sangb	bit, gravel, sand, clay, modal	1/31/90
08c	48970.2	102880.7	gamma40, sp, res_16, res_64, res_pt, gamma30, density, res_mg, cal30, gamma55, neu_api	bit, cec, toc,gravel, sand, clay, modal	2/7/90
09c	49015.6	102814.4	gamma40, sp, res_16, res_64, res_pt, temp, res_fl, gamma30, density, res_mg, cal30, gamma55, neu_api, sang, sangb	bit, gravel, sand, clay, modal	2/2/90
10c	49011.6	102892.3	gamma40, sp, res_16, res_64, res_pt, gamma30, density, res_mg, cal30, gamma55, neu_api, sang, sangb	bit, gravel, sand, clay, modal	2/6/90
17c	48706.9	102394.6	gr_api, sp, res_16, res_64, res_pt, caliper	gravel, sand, clay, modal	6/1/92
18c	48650.9	102486.1	gr_api, sp, res_16, res_64, res_pt, caliper	gravel, sand, clay, modal	5/20/92
19c	48699.1	102502.7	gr_api, sp, res_16, res_64, res_pt, caliper	gravel, sand, clay, modal	5/4/92
20c	48710.8	102589.3	gr_api, sp, res_16, res_64, res_pt, caliper	gravel, sand, clay, modal	6/11/92

Table A3. Core data from MHB-series of holes.			
MHB wells	East	North	Other Traces
1t	48773.4	102715.3	permv, permh, porv, porh, rhob, cec
4t	48875.6	102788.9	permv, permh, porv, porh, rhob, cec
5t	48919.0	102729.7	cec, toc
8t	48983.0	102886.6	cec, toc
3v	48874.1	102774.7	cec, toc

Table A4. Geophysical logs and other curves from AMH-series of holes.			
AMH wells	East	North	Logs
1	48744.2	102654.7	caliper
2	48807.8	102708.8	gammaray, sp, res_16, res_64

Table A5. Cone penetrometer logs acquired by Applied Research Associates during June - July, 1992. All holes contain sleevest, tipstunc, tipstcor, ratiocor, porepres, and res curves.

CPT number	East	North
1-	48761.5	104527.3
2-	47884.8	104243.6
3-	45819.4	103251.7
4-	45512.1	104120.5
5-	47863.3	103874.7
6-	48469.7	103064.8
7-	47586.2	102444.4
9-	47696.7	100993.0
10-	46714.6	100505.8
11-	46114.5	101349.2
12-	45036.4	103267.6
13a	45297.1	103066.8
13b	45312.2	103083.2
14-	46433.0	102736.3
15a	48778.9	102963.8
15b	48785.4	102957.8
17-	50104.1	101955.2
18a	48487.1	102198.8
18b	48511.1	102232.2
19a	48257.9	102264.5
19b	48250.5	102268.8
20a	47921.3	102448.2
20b	47906.8	102500.2
21-	48590.5	101383.0
22-	48316.8	102495.9
23a	46704.5	103862.0
23b	46596.2	103812.5

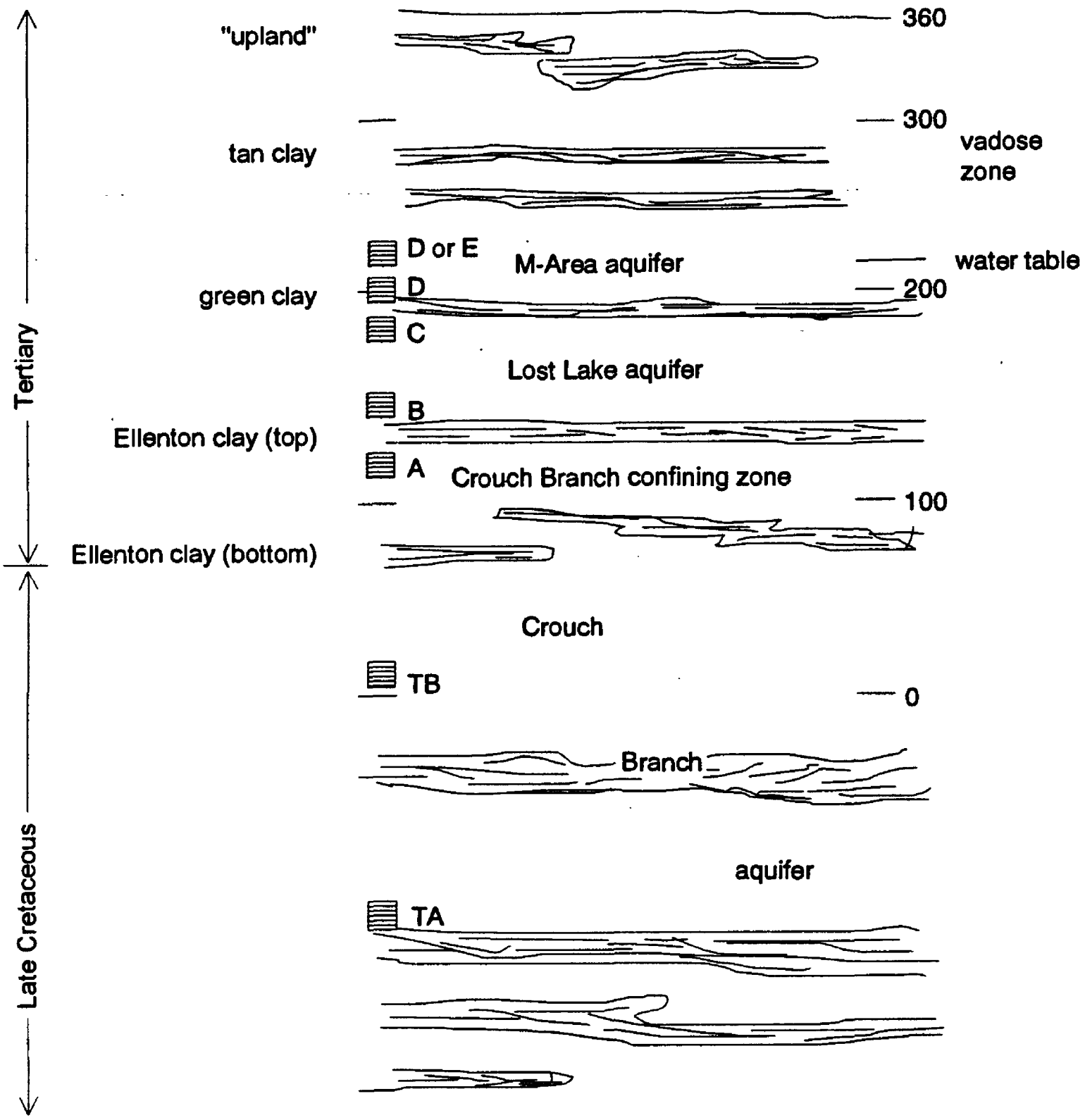

Figure 1. Sketch of sand (open) and clay (lined) layering in upper 550 feet of the A/M area. Also shown are hydrogeologic units, water table at interface between vadose zone and semiconfined zone of the M-area aquifer, and typical placement of well screens TA through E. Elevation (feet) is with respect to mean sea level.

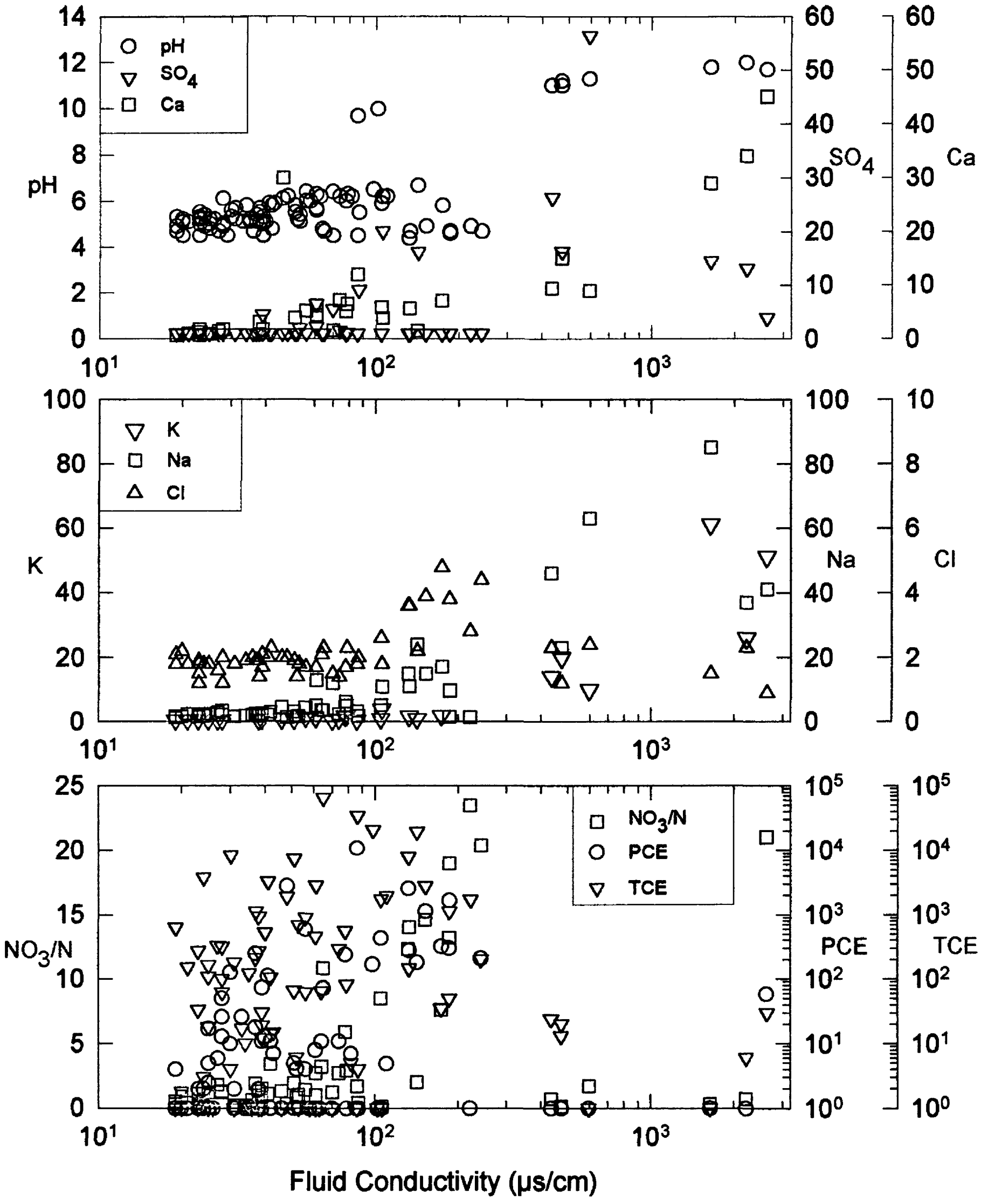

Figure 2. Major ions (mg/L), pH, and concentrations of PCE and TCE (μg/L) in water samples from the Lost Lake aquifer. High pH samples are attributed to leaching of cement.

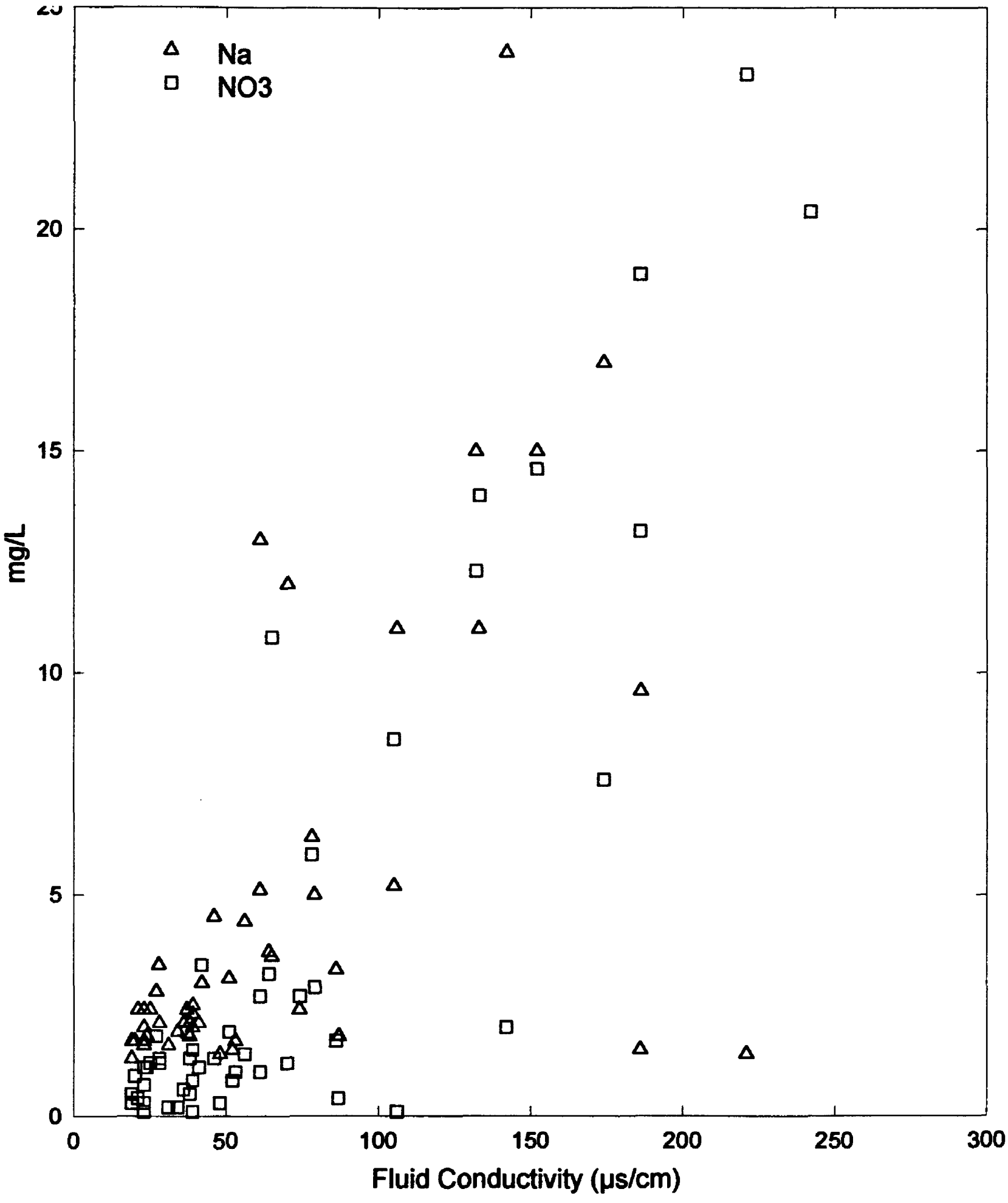

Figure 3. Sodium and nitrate concentrations (mg/L) in water samples from the Lost Lake aquifer, limited to samples with fluid conductivity less than 300 μS/cm.

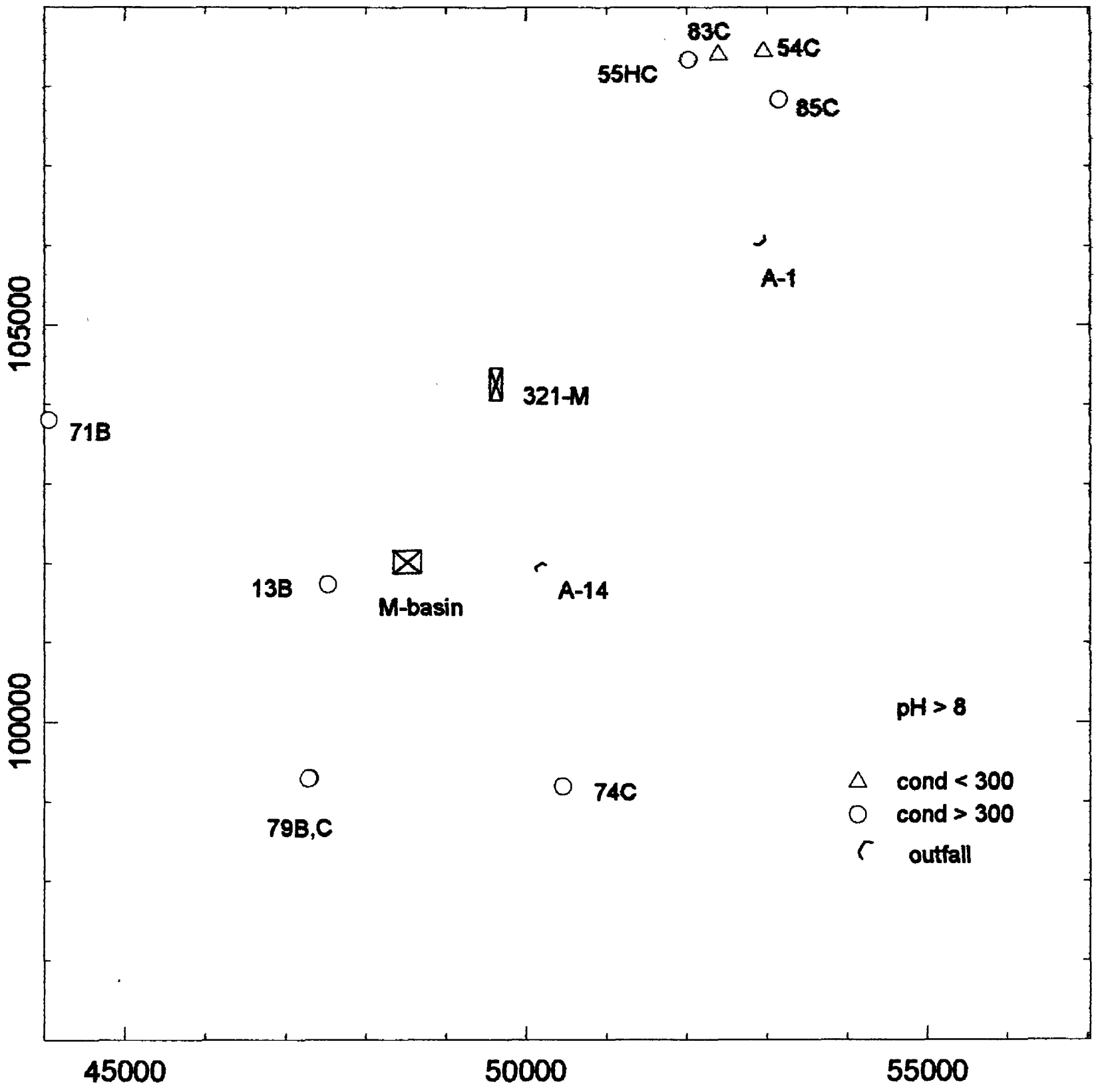

Figure 4. Map of the A/M area showing wells with pH greater than 8 in water samples from the Lost Lake aquifer. Two wells have samples with conductivity less than 300 μS/cm. High pH is attributed of cement in the wellbore.

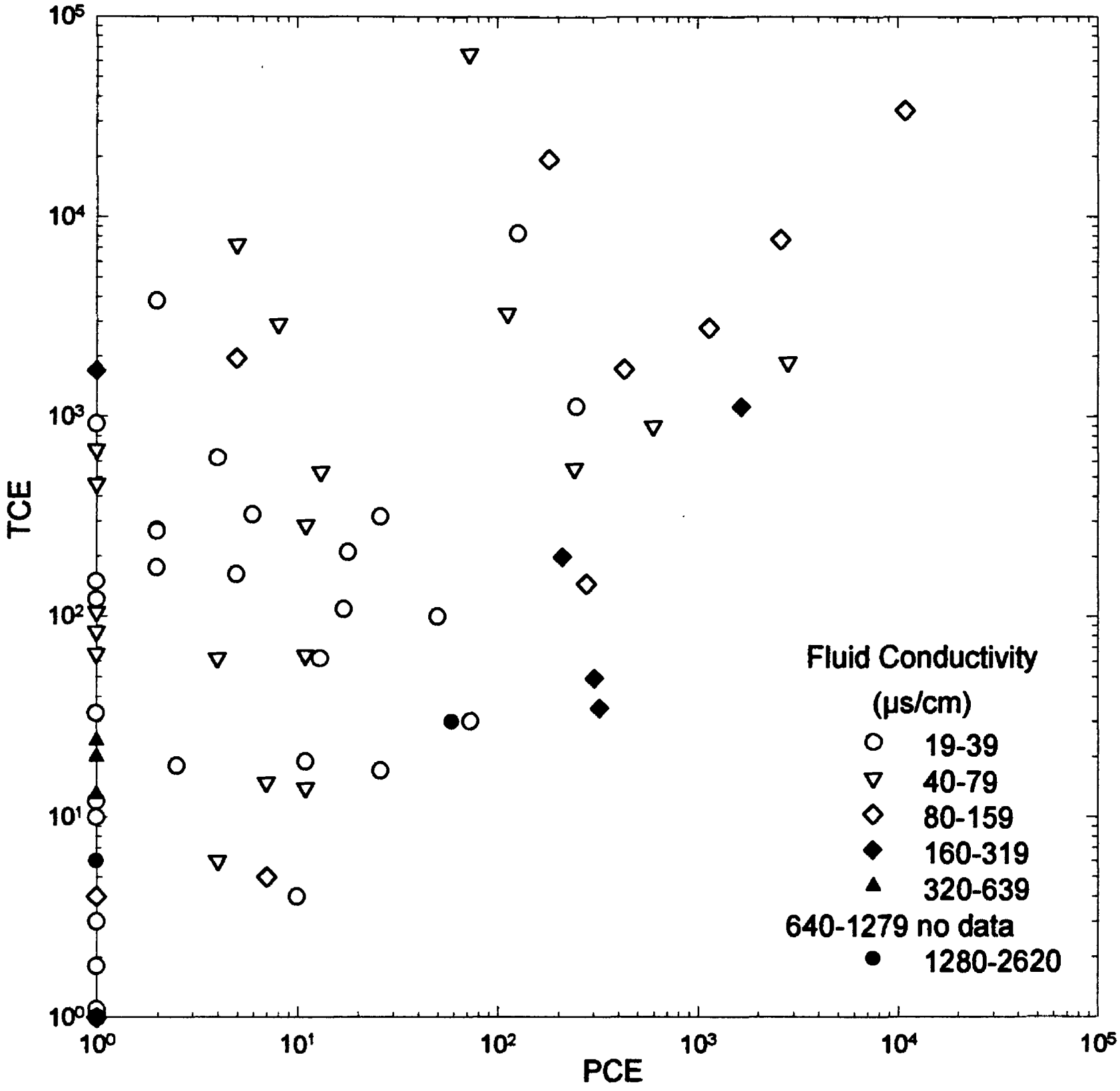

Figure 5. Values of trichloroethylene (TCE) versus tetrachloroethylene (PCE) from water well samples.

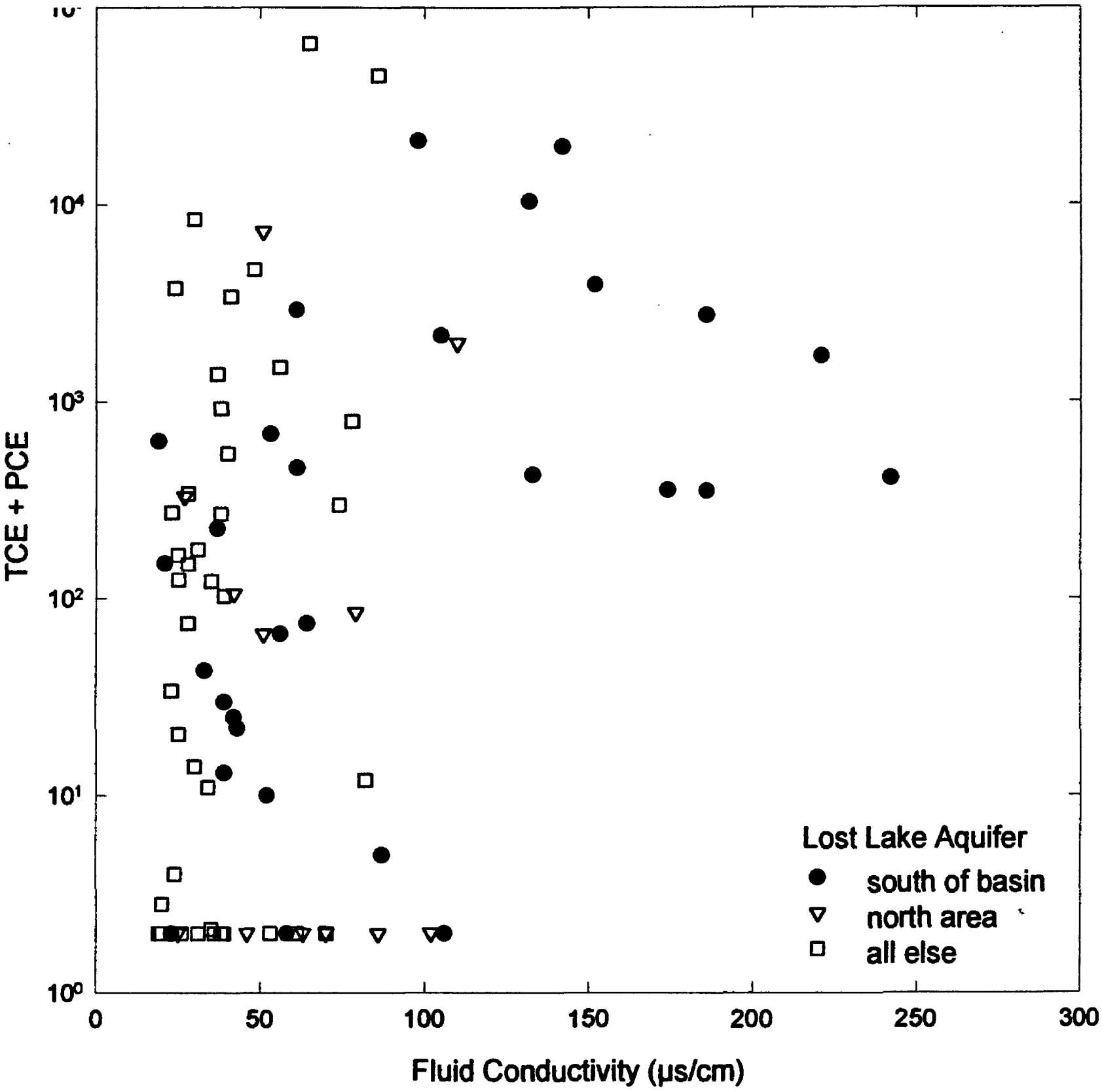

Figure 6. Summed values of trichloroethylene (TCE) and tetrachloroethylene (PCE) versus conductivity from water well samples from the Lost Lake aquifer.
South of basin: North < 101,868 and (North < 103,500.and.East < 47,600).
North area: (North > 106,700.and.East > 51,400).

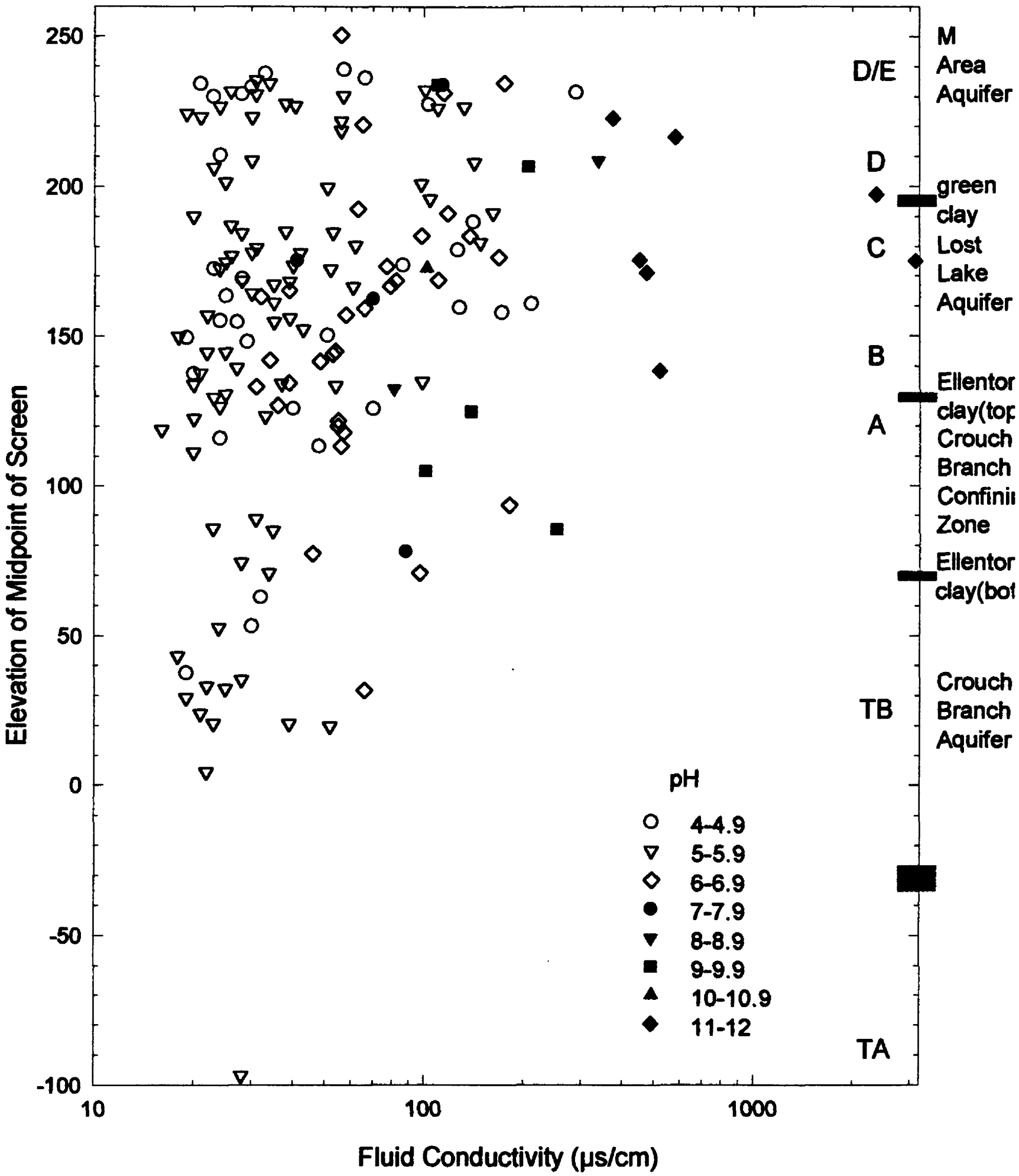

Figure 7. Fluid conductivity of water samples as a function of sample elevation, for varying pH. Letters TA through D/E indicate nominal elevations of well screens.

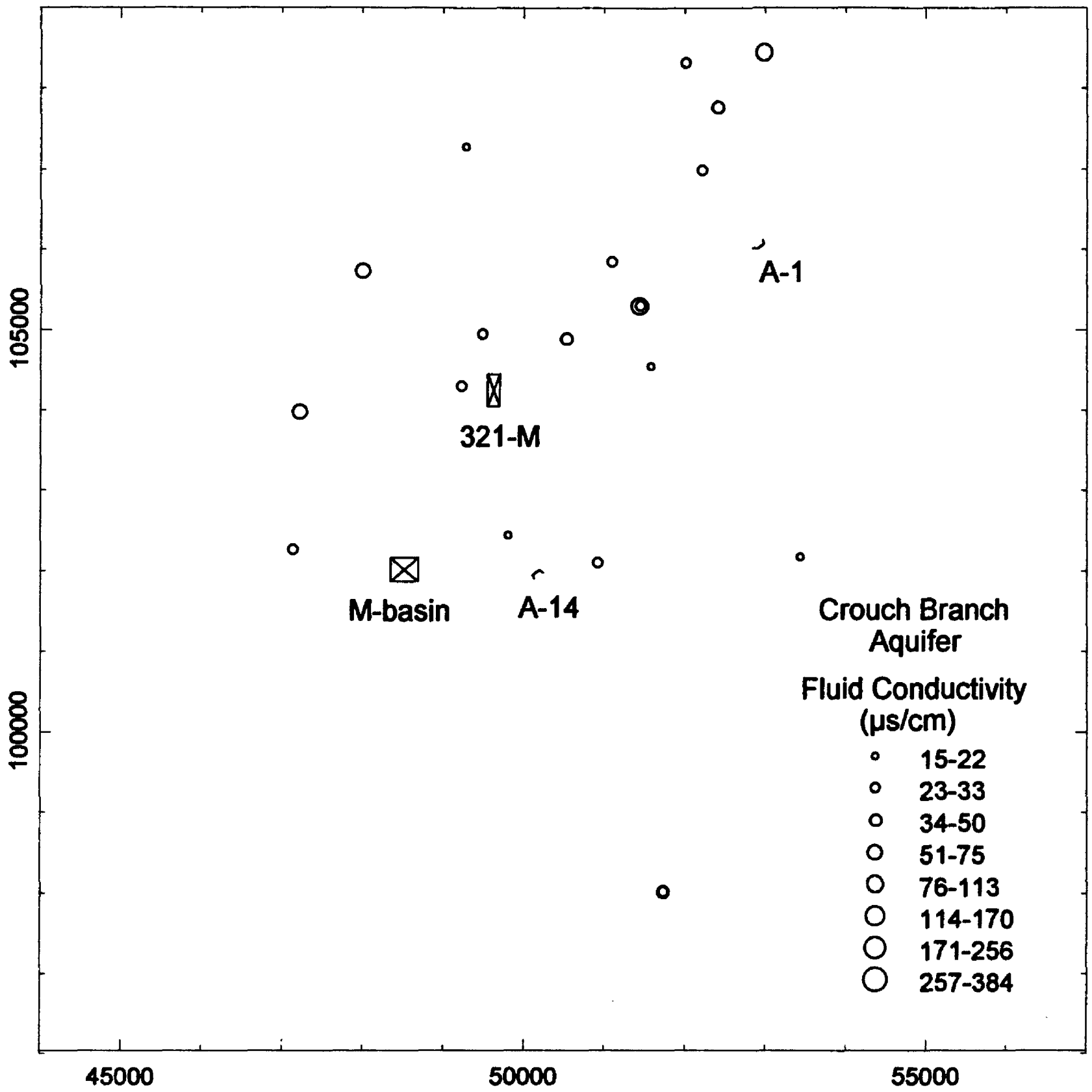

Figure 8. Map of the A/M area showing distribution of fluid conductivity (μS/cm) of water samples obtained from screened zones in the Black Creek unit, also referred to as the Crouch Branch aquifer. Square with X is the settling basin, rectangle with X is building 321-M. Fluid conductivity ranges are spaced logarithmically, with the upper end of a range 1.5 times the lower end. Samples with pH > 8 have been excluded.

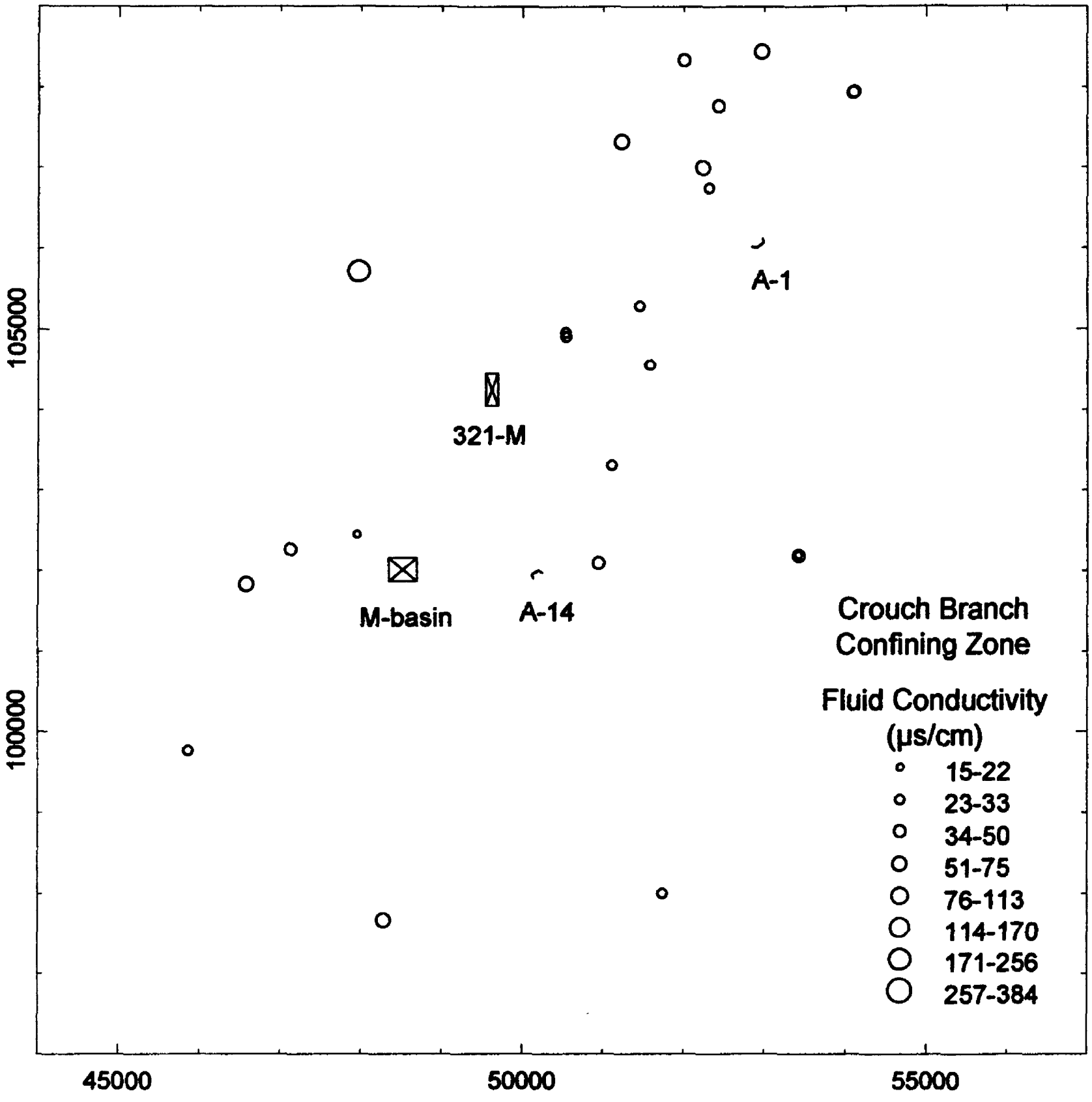

Figure 9. Map of the A/M area showing distribution of fluid conductivity (μS/cm) of water samples obtained from screened zones in the middle of the Crouch Branch confining zone, also referred to as the Ellenton Sand. Square with X is the settling basin, rectangle with X is building 321-M. Fluid conductivity ranges are spaced logarithmically, with the upper end of a range 1.5 times the lower end. Samples with pH > 8 have been excluded.

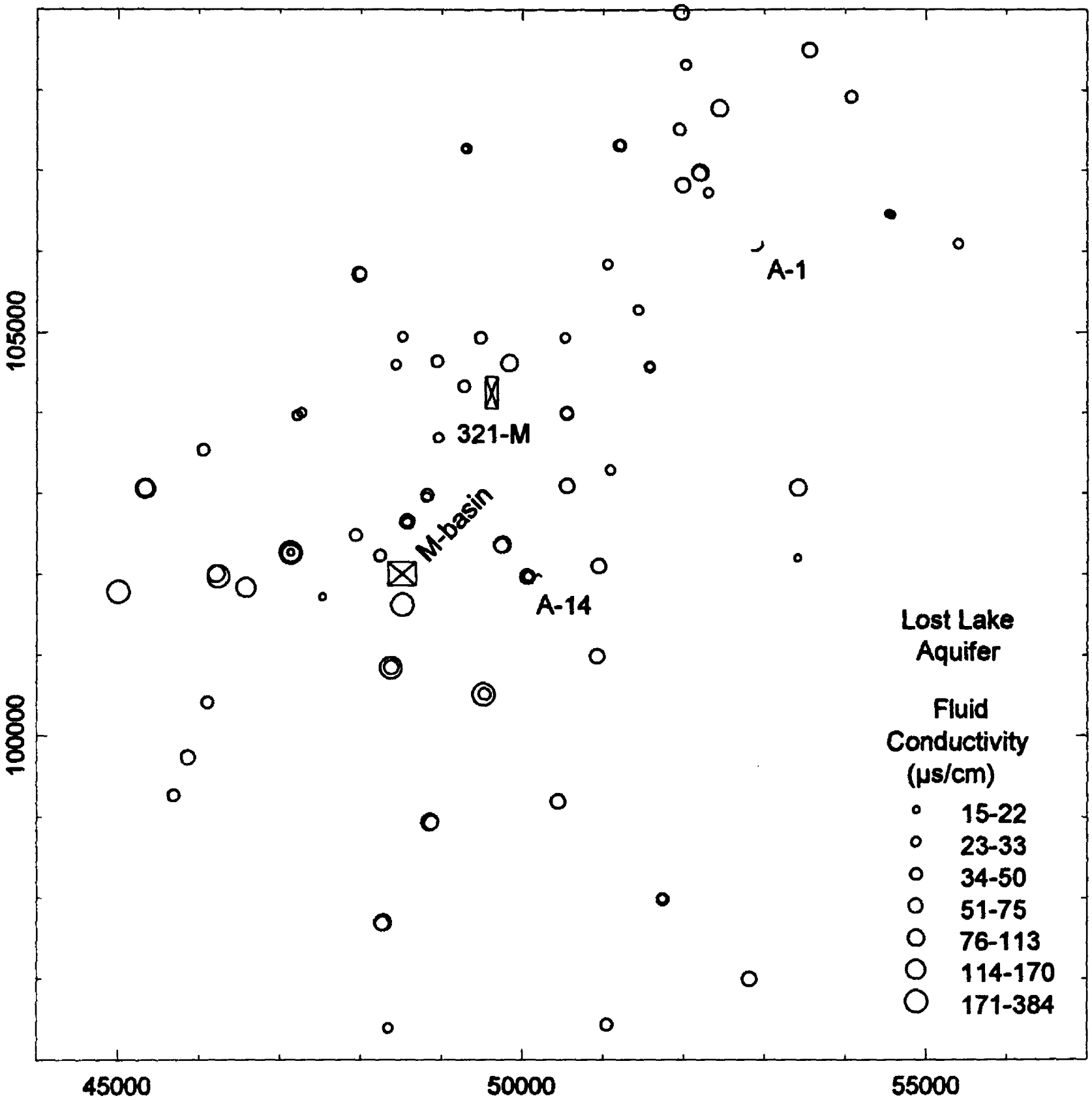

Figure 10. Map of the A/M area showing distribution of fluid conductivity (μS/cm) of water samples obtained from screened zones in the upper and lower Lost Lake aquifer below the green clay. Square with X is the settling basin, rectangle with X is building 321-M. Fluid conductivity ranges are spaced logarithmically, with the upper end of a range 1.5 times the lower end. Samples with pH > 8 have been excluded.

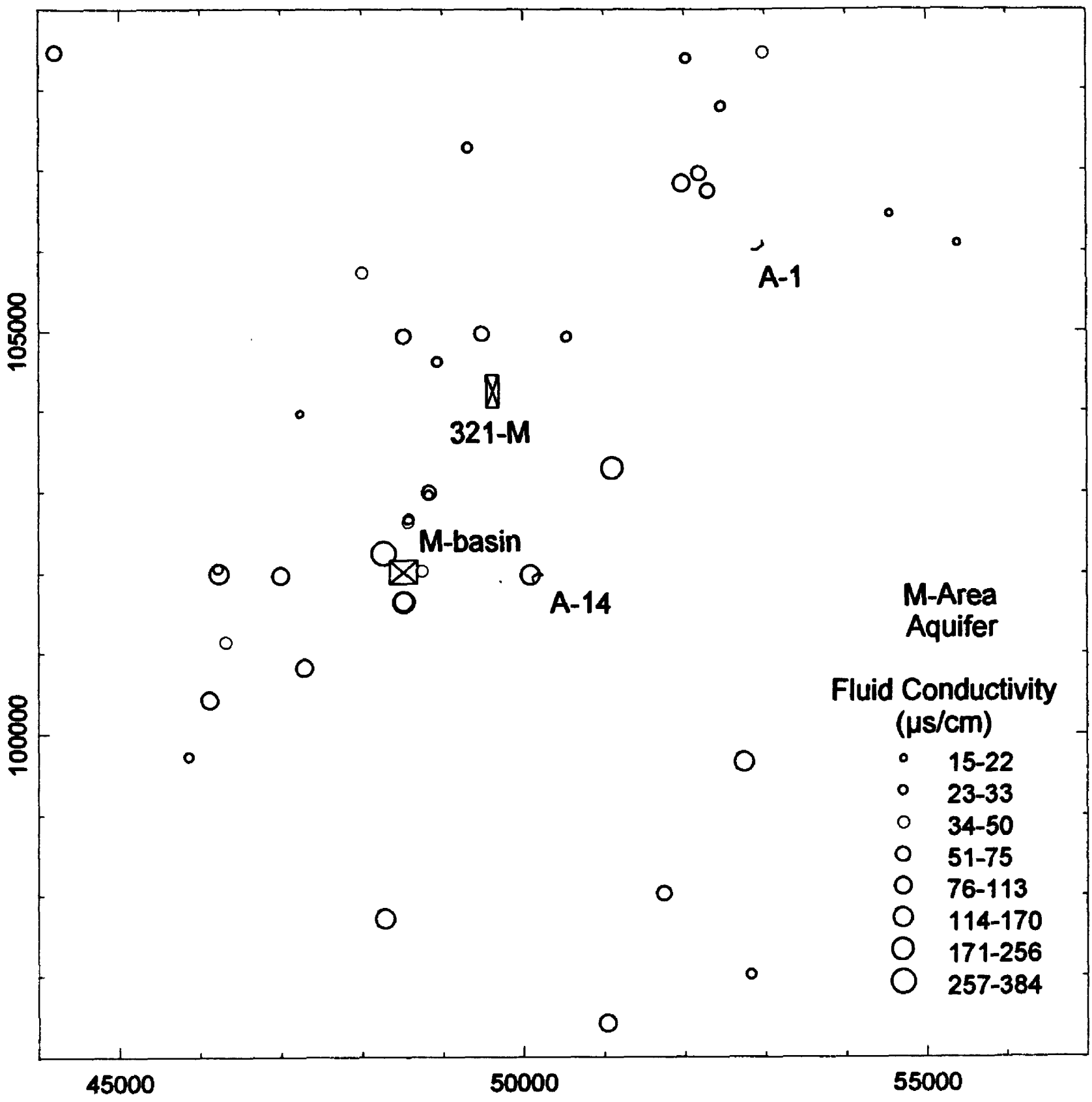

Figure 11. Map of the A/M area showing distribution of fluid conductivity (μS/cm) of water samples obtained from screened zones in the M-area (W.T.) aquifer above the green clay. Some screened intervals are in the vadose zone and some penetrate the green clay. Square with X is the settling basin, rectangle with X is building 321-M. Fluid conductivity ranges are spaced logarithmically, with the upper end of a range 1.5 times the lower end. Samples with pH>8 have been excluded.

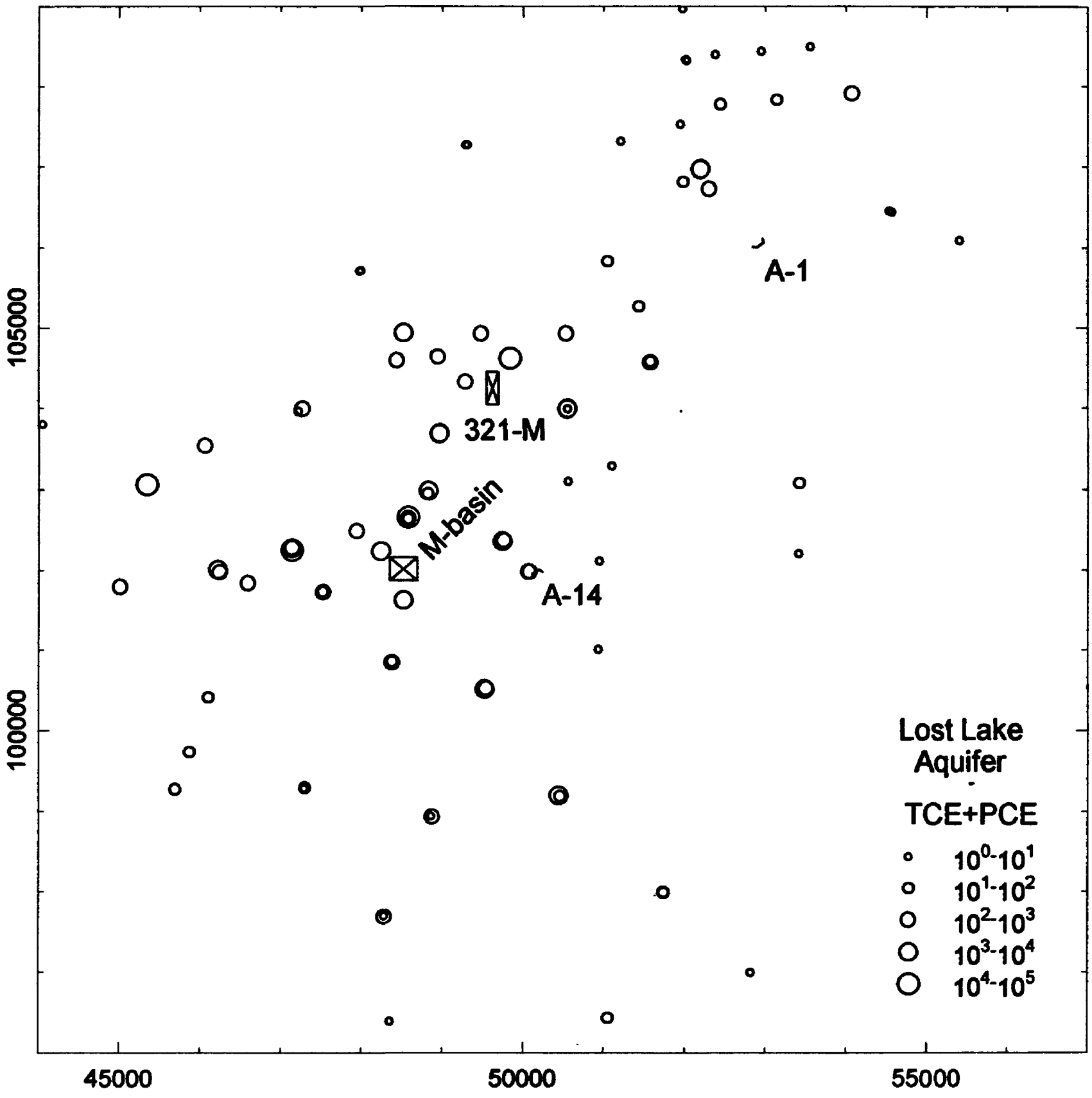

Figure 12. Map of the A/M area showing summed concentration (μg/L) of TCE and PCE in water samples from the Lost Lake aquifer.

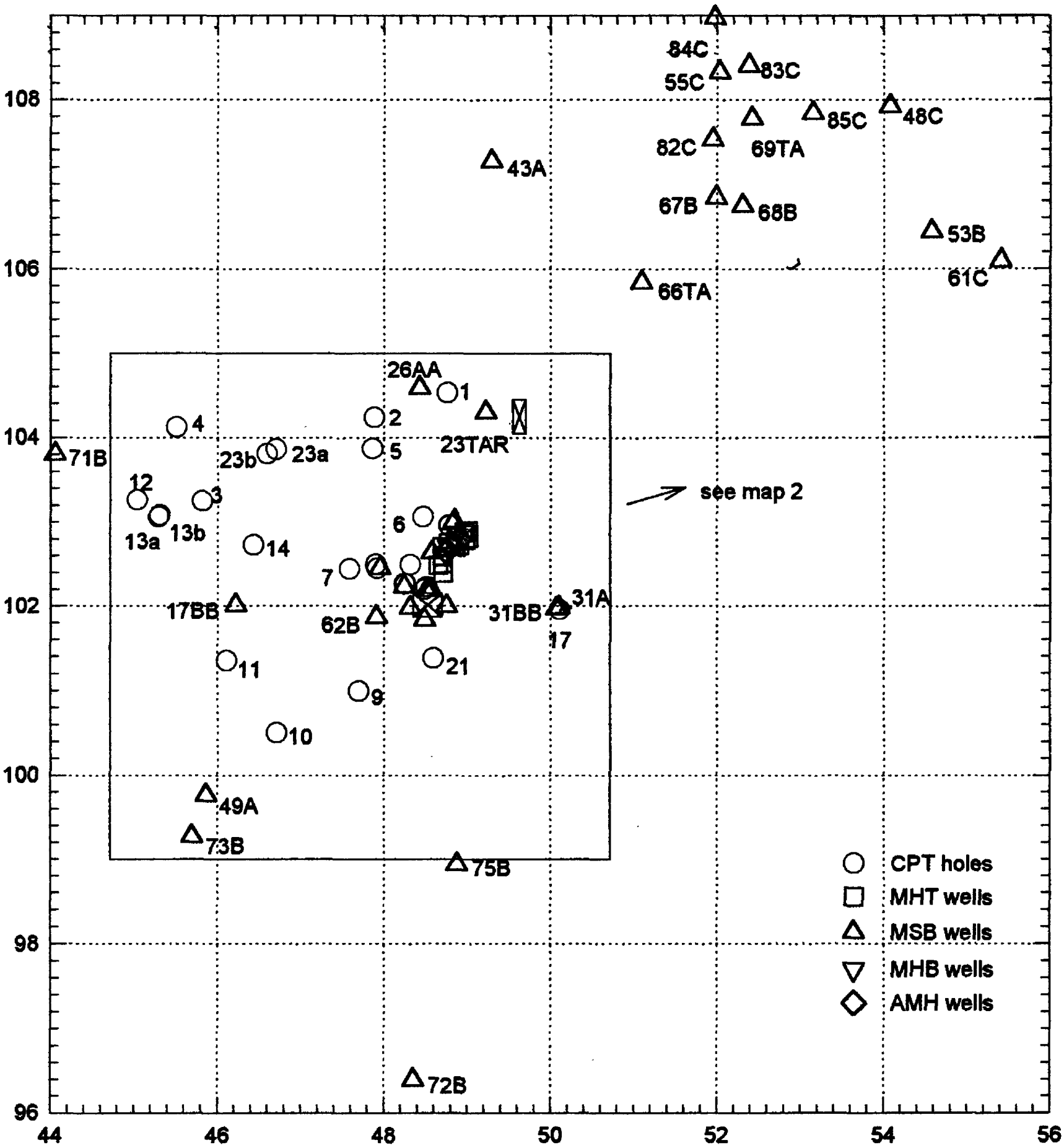

Figure 13. Map of A/M area showing locations of geophysical logs and penetrometer runs. Square with X is the settling basin, rectangle with X is building 321-M. SRS coordinate grid units in thousands of feet.

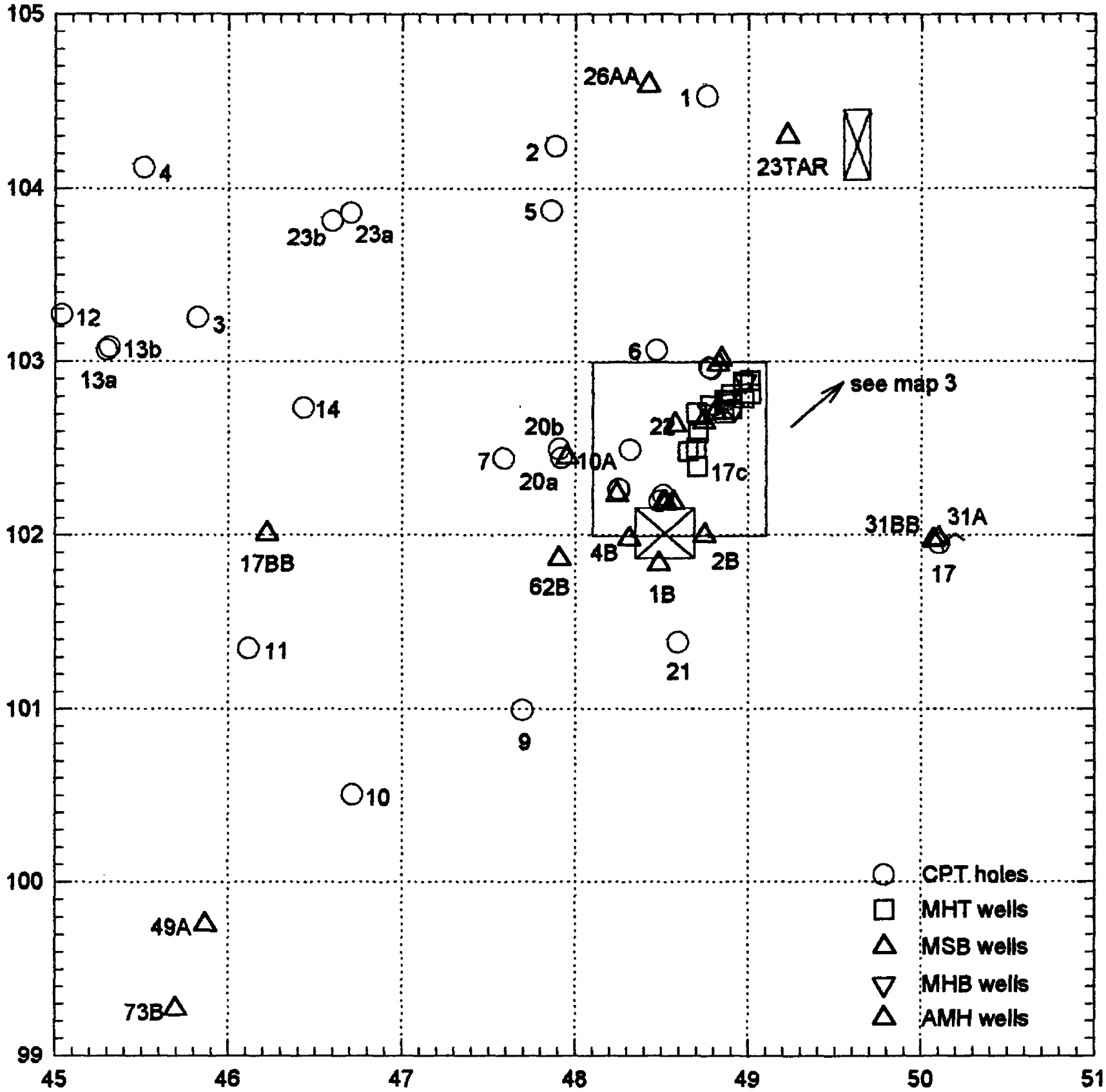

Figure 14. Insert map for figure 13 showing locations of geophysical logs and penetrometer runs. Square with X is the settling basin, rectangle with X is building 321-M. SRS coordinate grid units in thousands of feet.

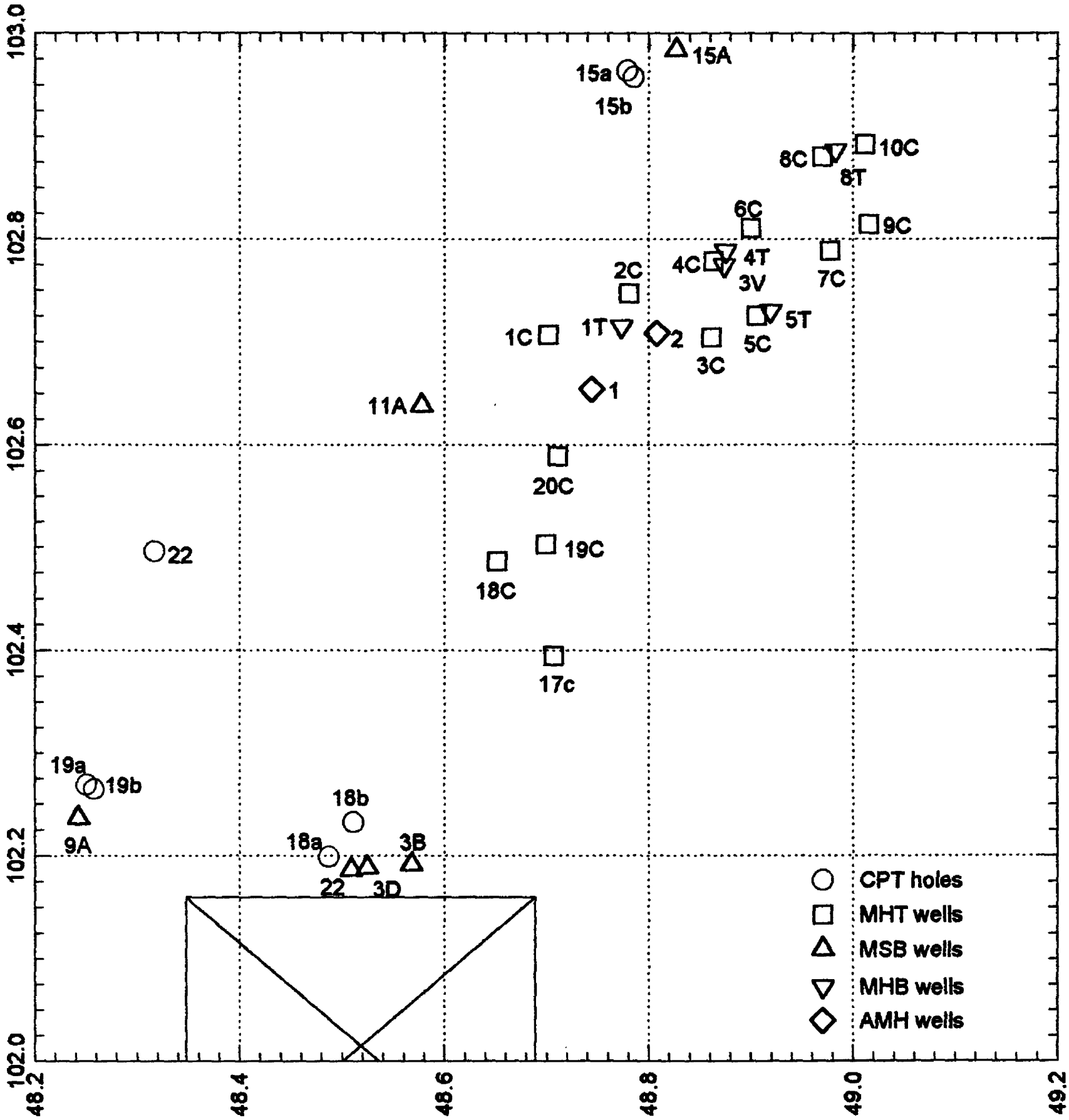

Figure 15. Inset map for figure 14 showing locations of geophysical logs and penetrometer runs on north side of settling basin. SRS coordinate grid units in thousands of feet.

Well Name: MSB-1B

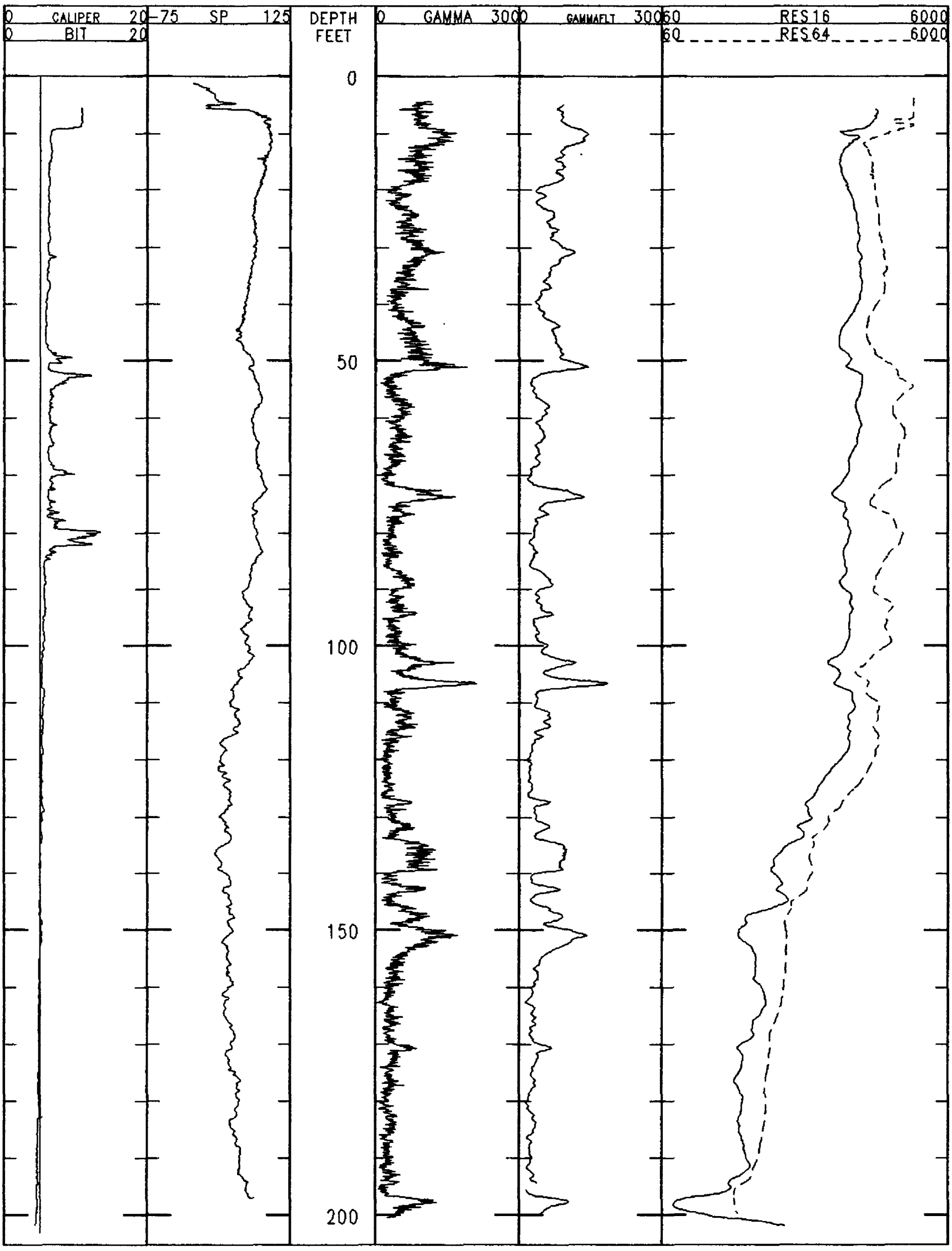

Figure 16. Example of standard open-hole logs from MSB-1B. From left to right: caliper and bit size, SP, gamma ray, filtered gamma ray, and resistivity from 16 and 64-inch normal.

Well Name: cpt007a

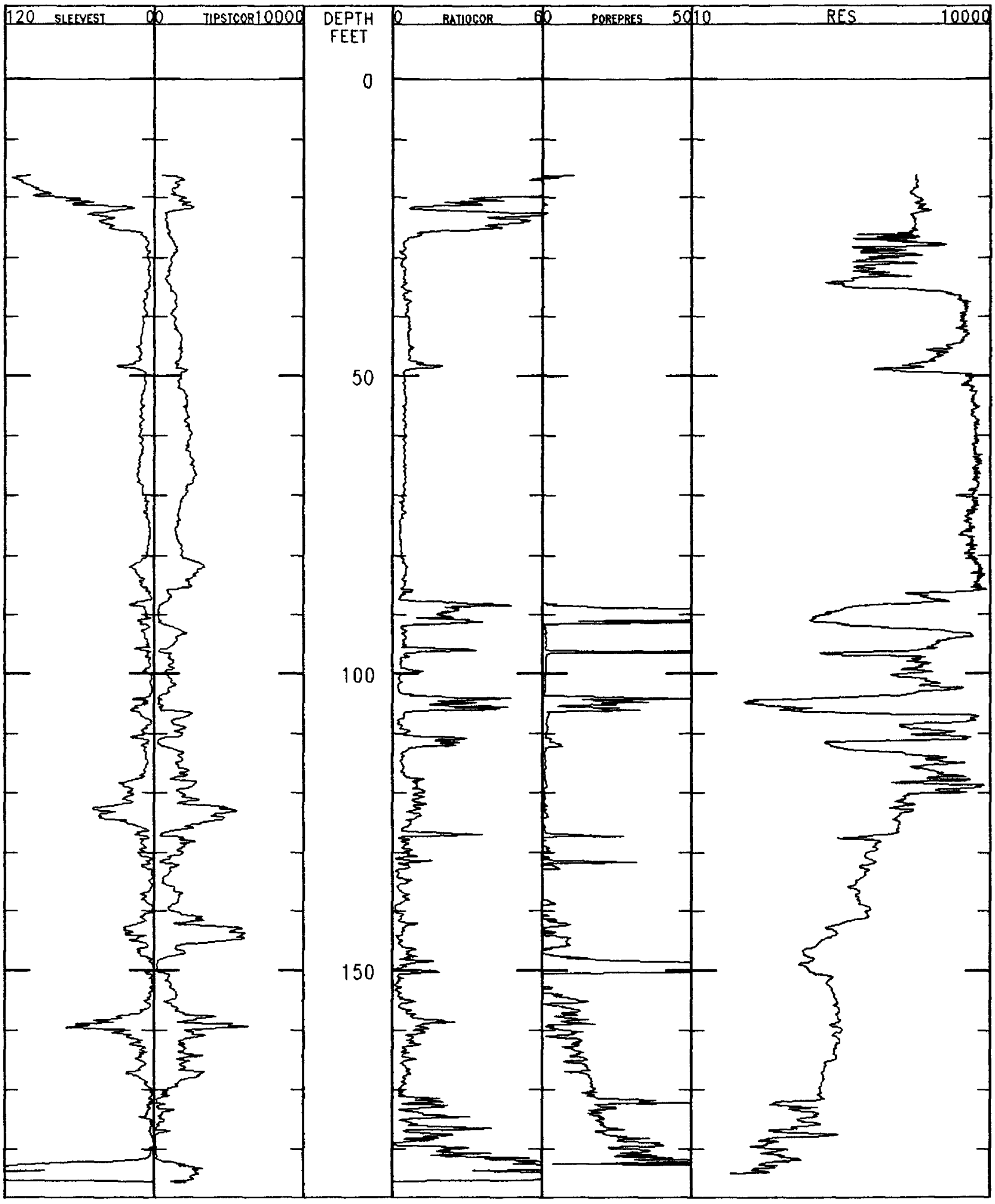

Figure 17. Cone penetrometer logs in CPT-007a. From left to right: sleeve stress, tip stress, ratio of sleeve stress to tip stress, pore pressure, and electrical resistivity. See Table 8 for units. Resistivity scale is logarithmic and spans three decades.

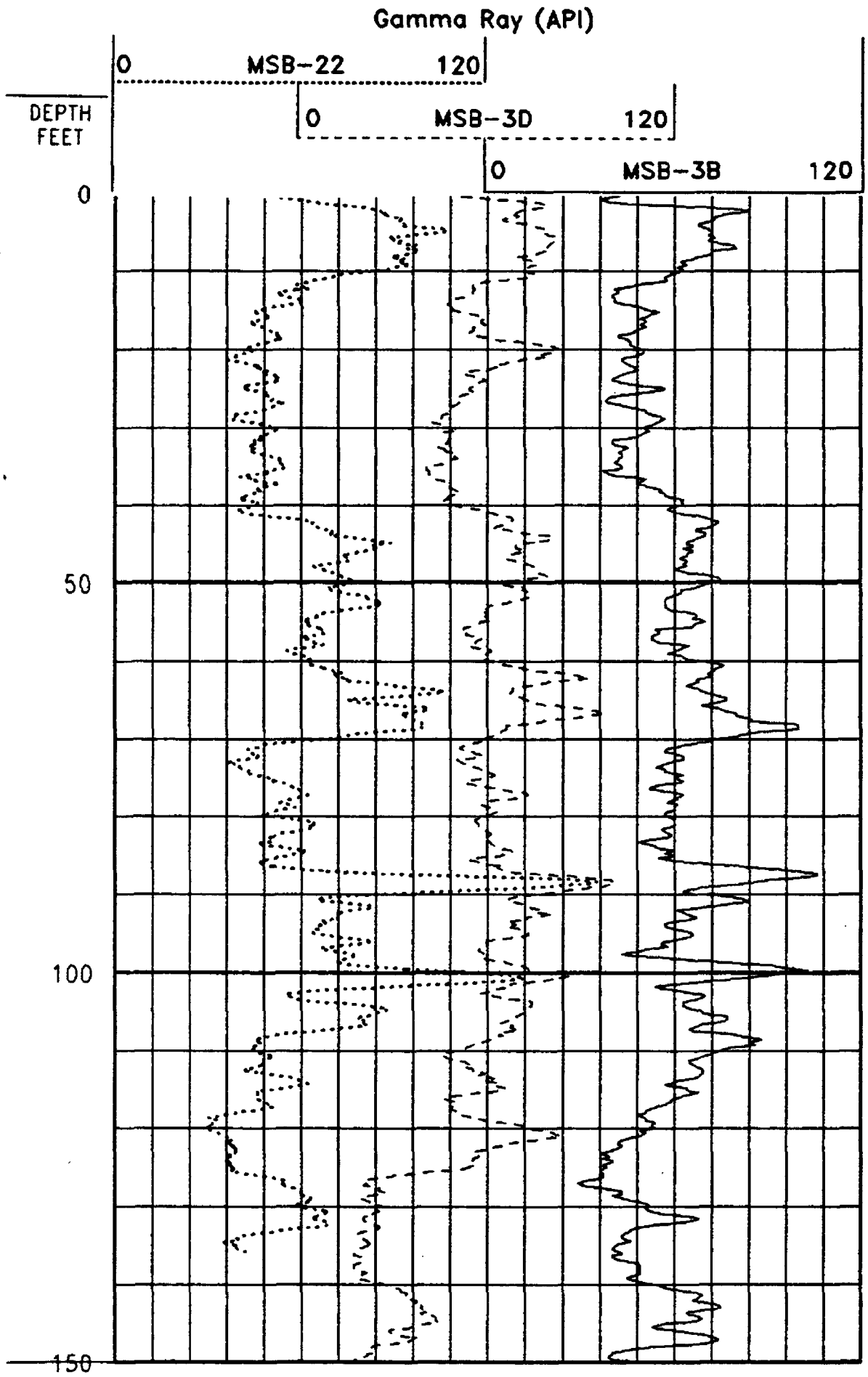

Figure 18. Gamma-ray logs within grouted 4-inch PVC casing in MSB-3B, MSB-3D, and MSB-22, all located within 60 feet of one another on north side of settling basin.

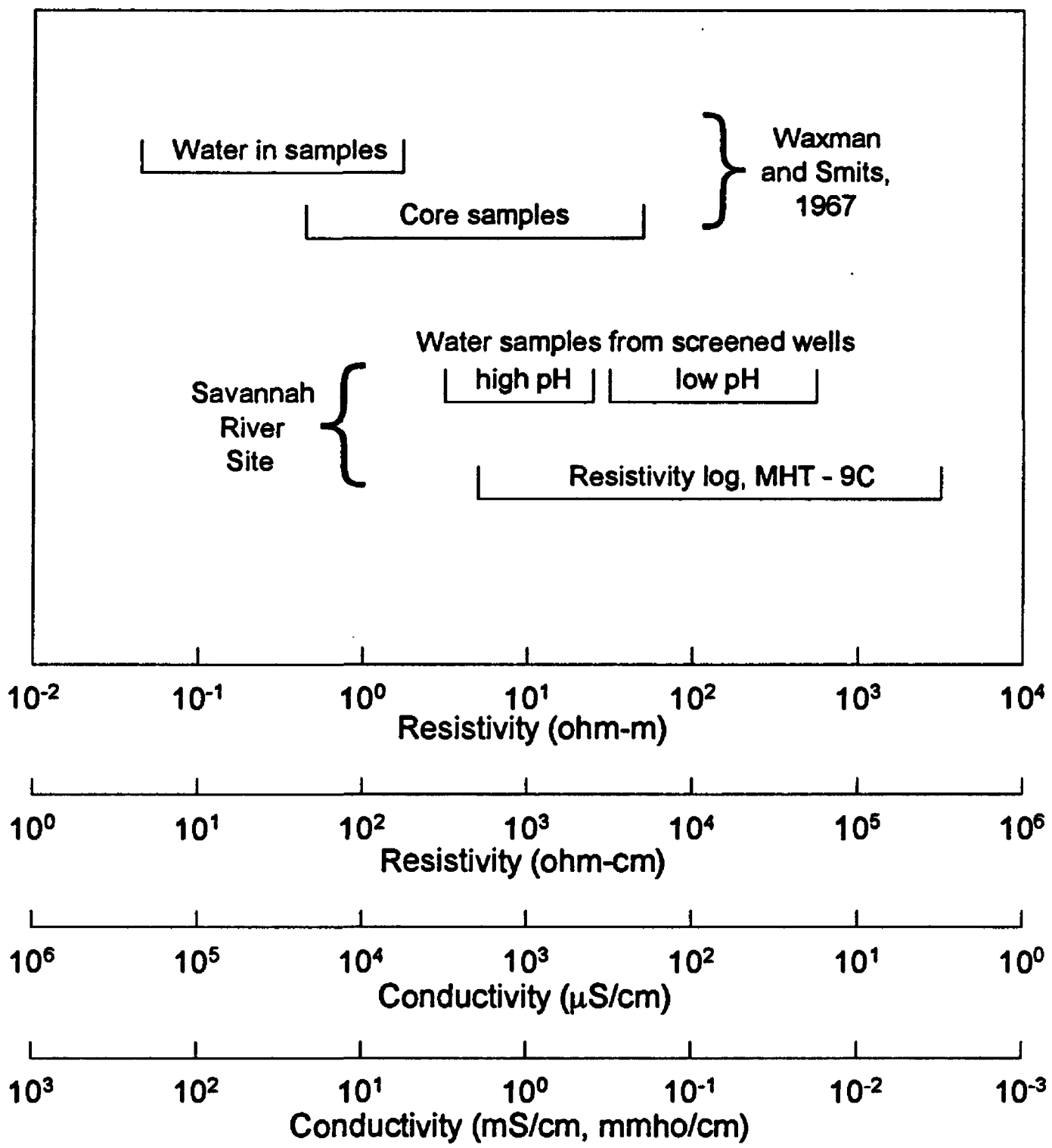

Figure 19. Ranges of electrical resistivity (conductivity) of core samples and saturant used by Waxman and Smits (1967), and ranges for water samples and a resistivity log from the A/M area.

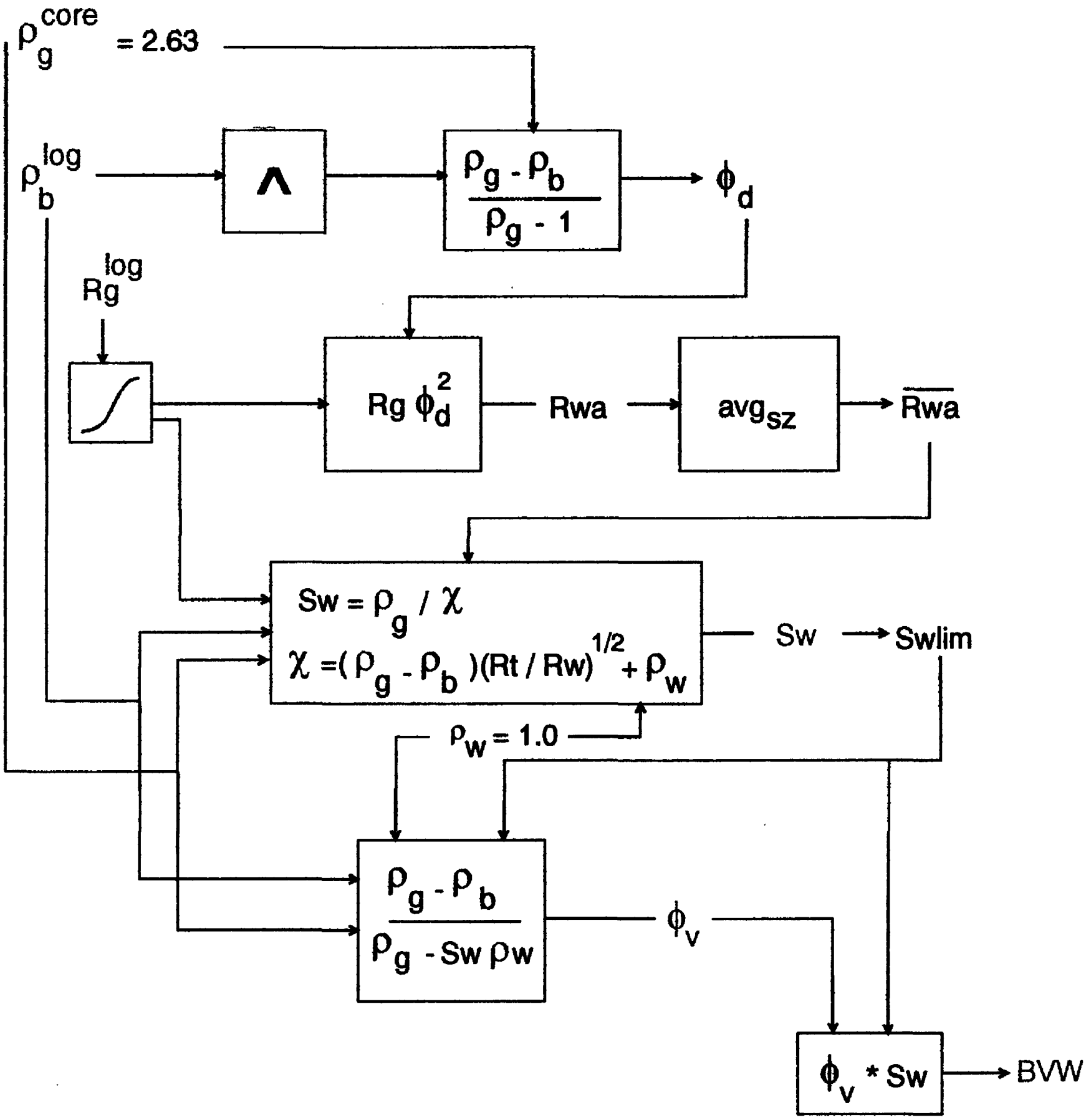

Figure 20. Sequence of steps for computing saturation, porosity, and water content in the vadose zone. Top row: grain density is assigned a value of 2.63 g/cm^3. Second row: density log is smoothed and used with grain density to compute porosity in saturated zone. Third row: resistivity log from guard tool is corrected, then used to compute apparent water resistivity; an average water resistivity is obtained from a depth interval in the saturated zone. Fourth row: Saturation is computed from four inputs and is constrained to not exceed a value of 1.0. Fifth row: Porosity in the vadose zone is computed from four inputs. Sixth row: water content Bvw is computed from porosity and saturation.

Well Name: MHT-9C

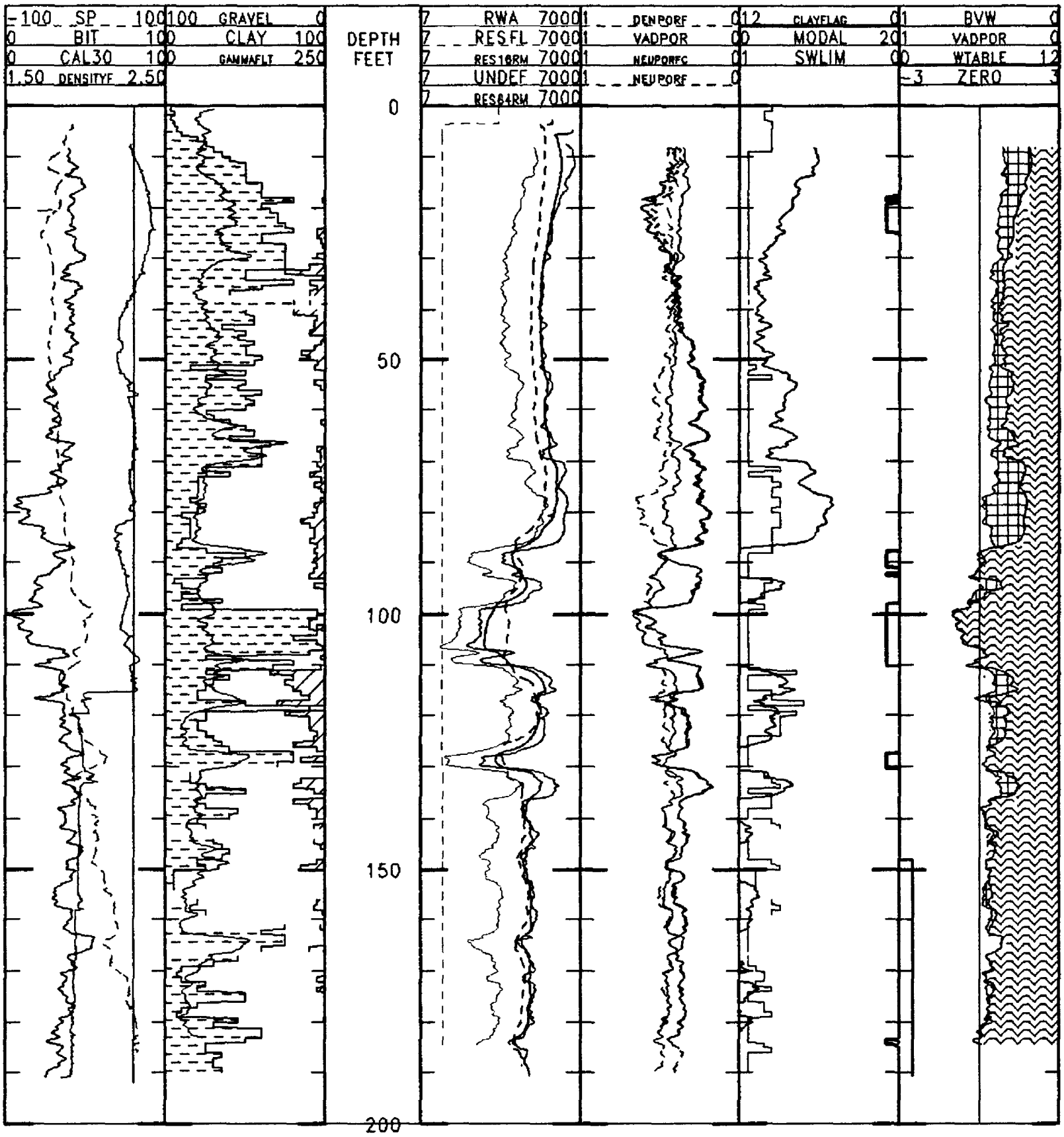

Figure 21. Original and computed log curves for well MHT-9C. Original curves, with filtering and borehole corrections, are shown in three lefthand columns, except for Rwa. Computed curves (see Table 10) include most of those in the three righthand columns, except Wtable and Modal. Column 6 (rightmost column) shows porosity at less than 0.5 throughout most of hole; red waffle grid shows air-filled porosity and blue wavy pattern shows water-filled porosity. Water table lies at 148 feet subsurface.

Well Name: MHT-1C

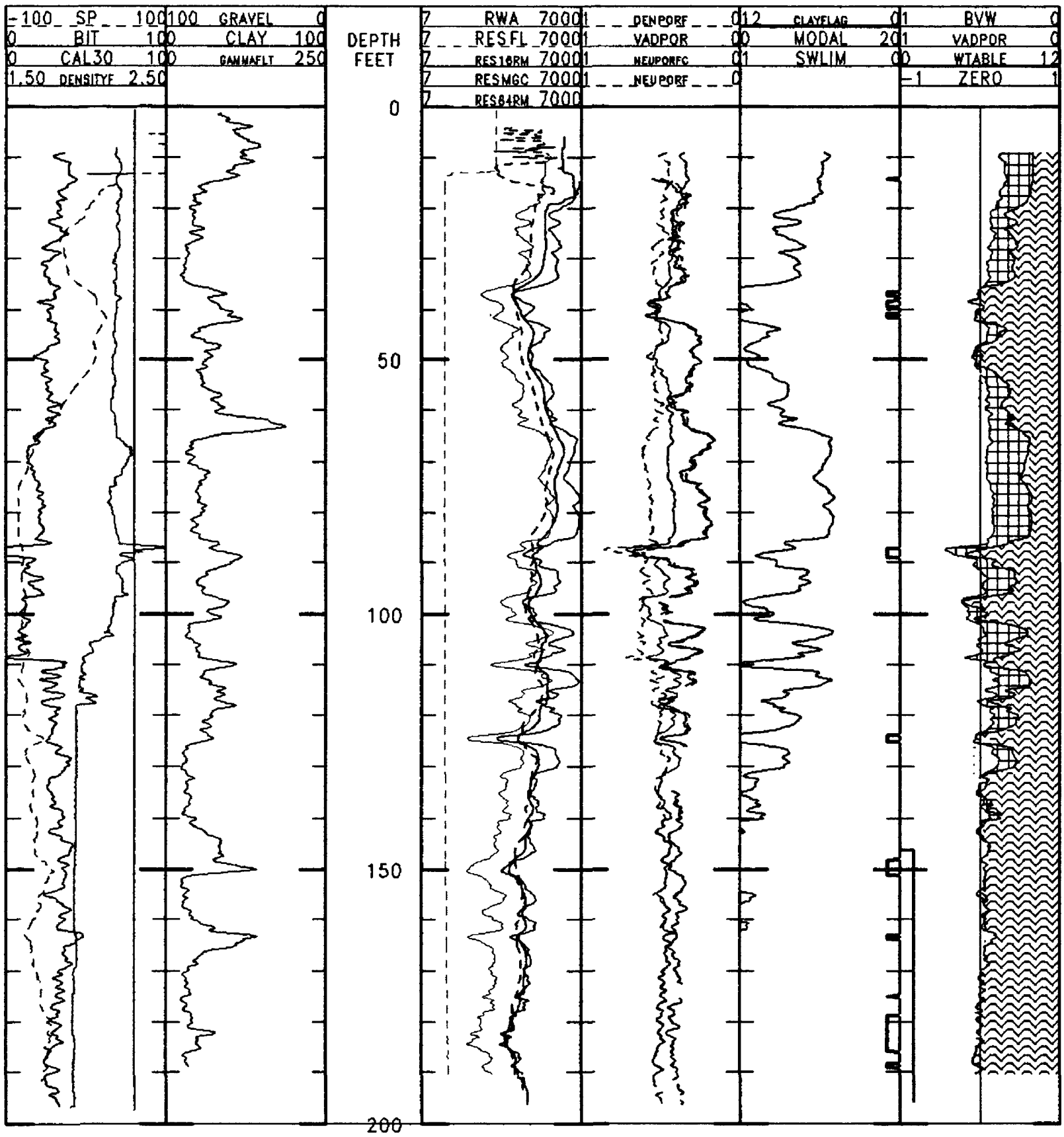

Figure 22. Original and computed log curves for well MHT-1C.

Well Name: MHT-3C

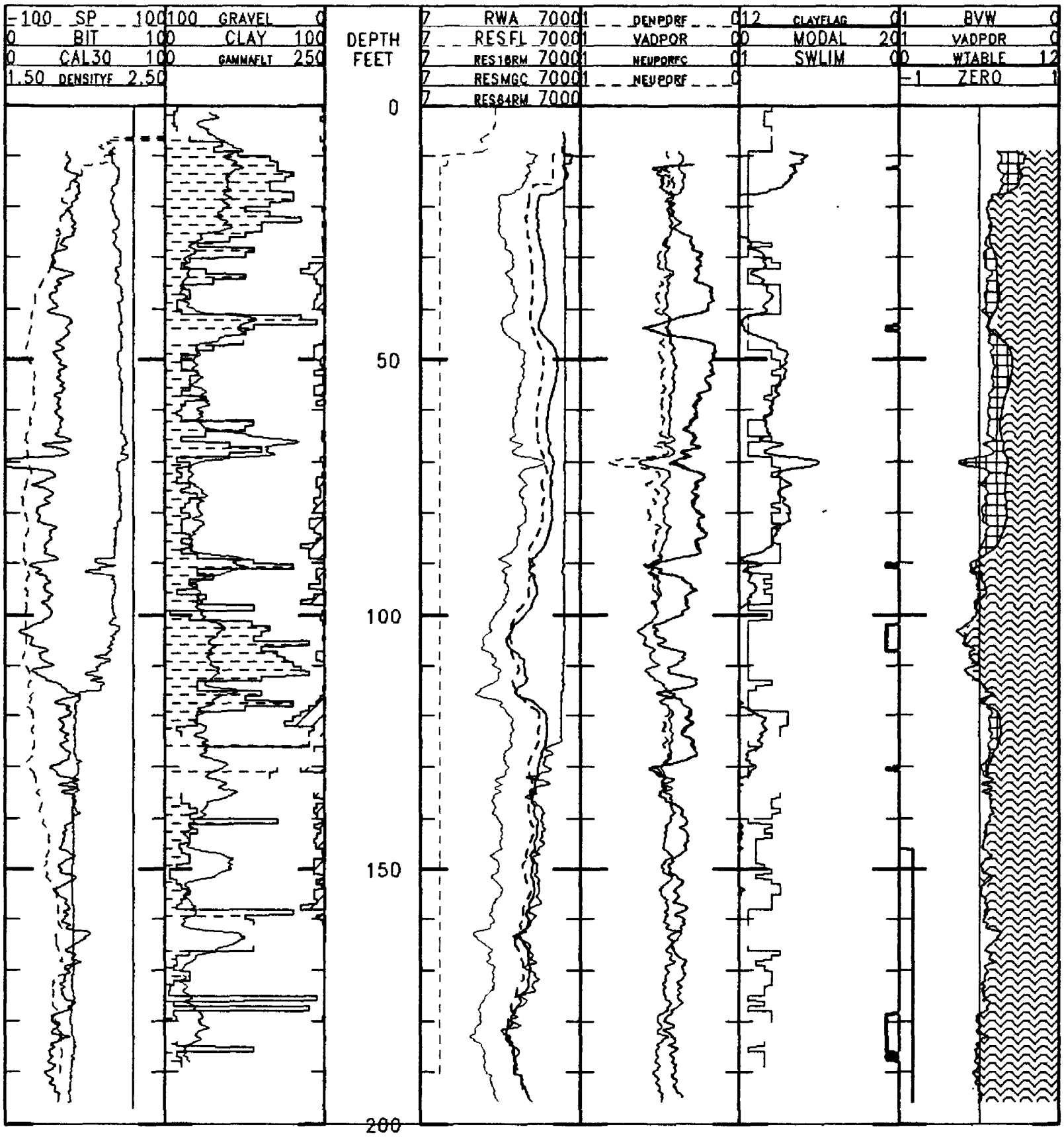

Figure 23. Original and computed log curves for well MHT-3C.

Well Name: MHT-7C

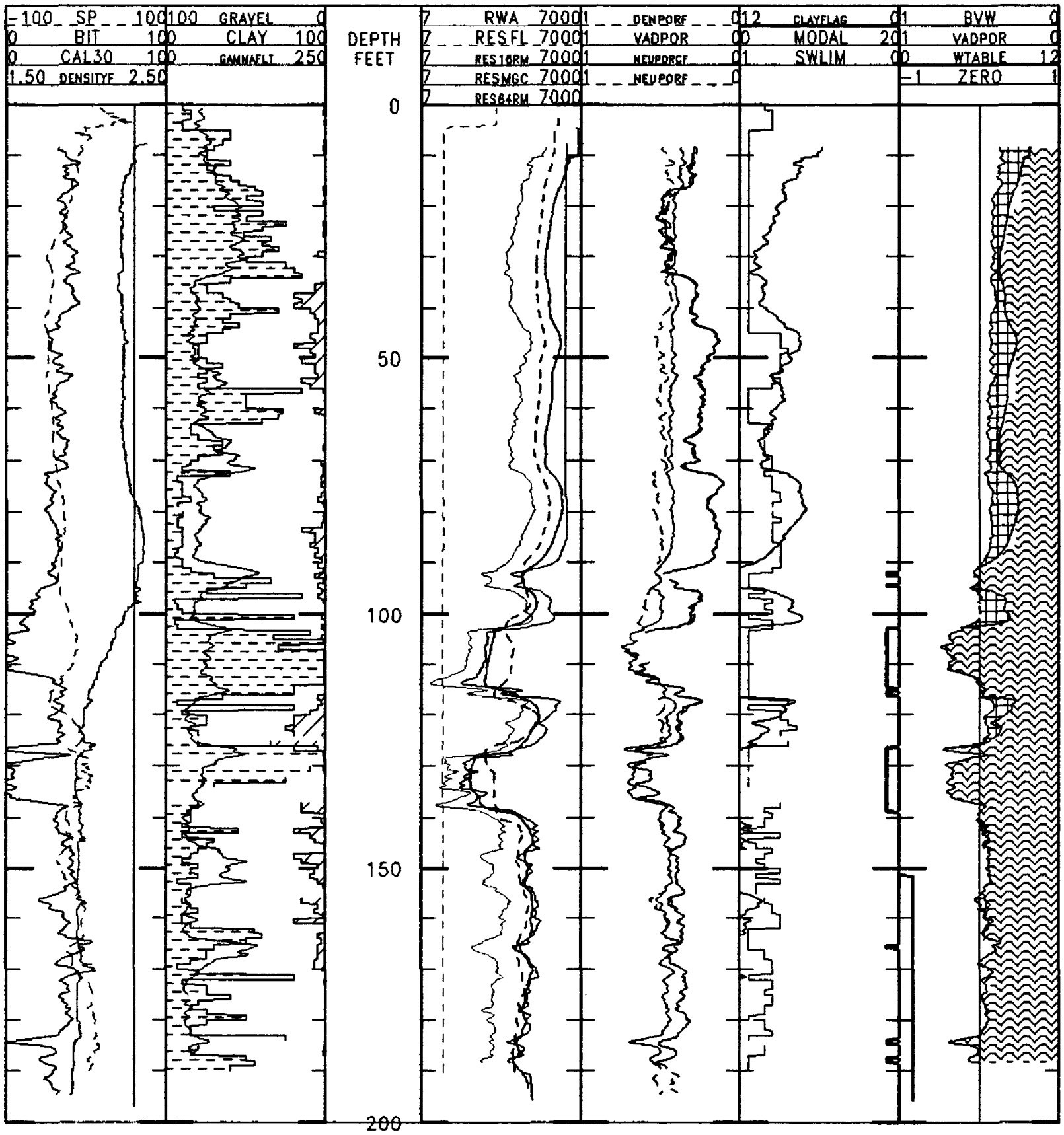

Figure 24. Original and computed log curves for well MHT-7C.

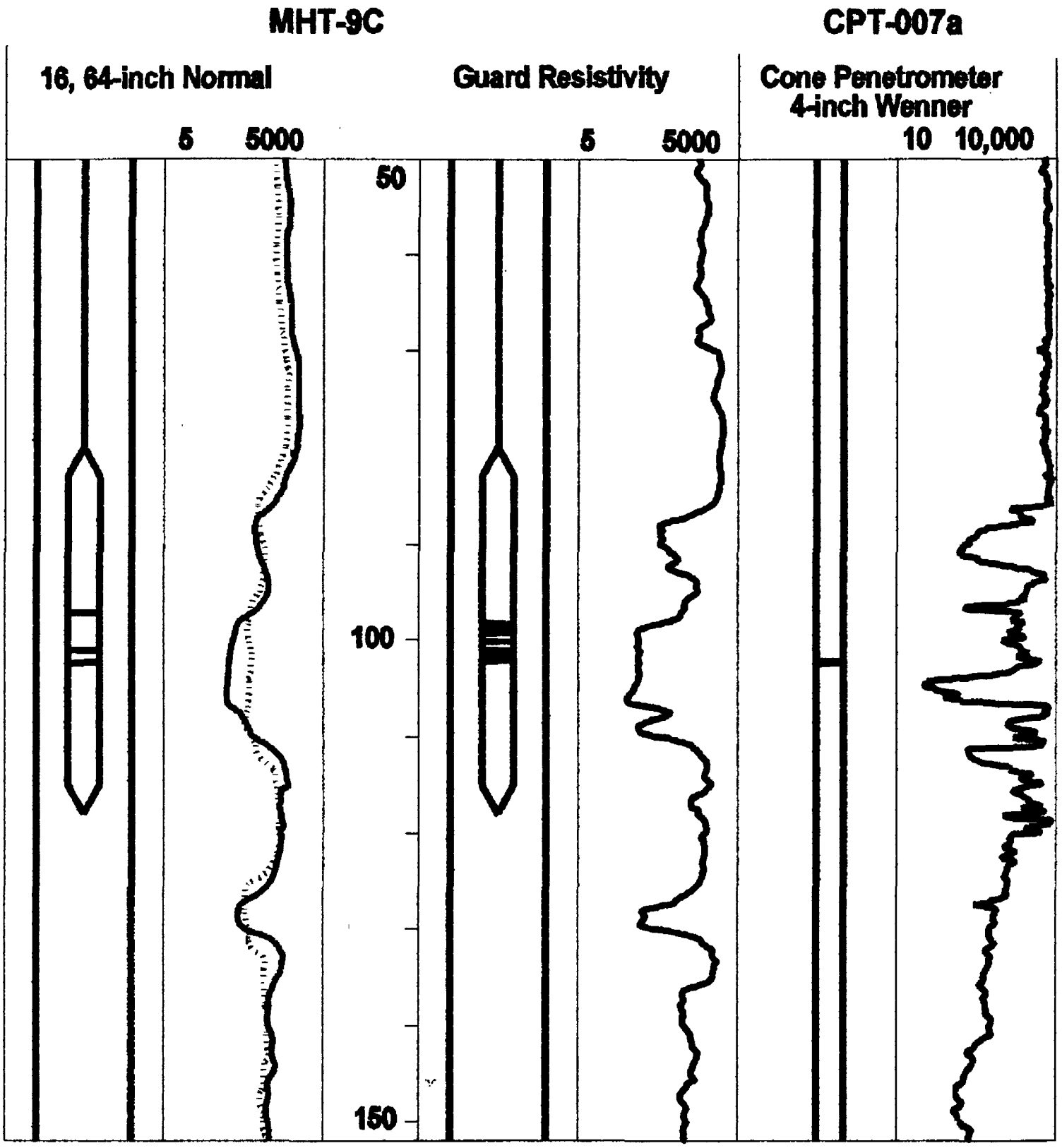

Figure 25. Resistivity sensors and logs illustrating resolution of normal (16-inch curve is solid, 64-inch curve is dashed), guard, and penetrometer tools. Electrode spacings are true to the depth scale in feet, but the tool lengths are not. Scales in ohm-m are logarithmic. Normal and guard examples are both from MHT-9C, penetrometer example is from CPT-007a.

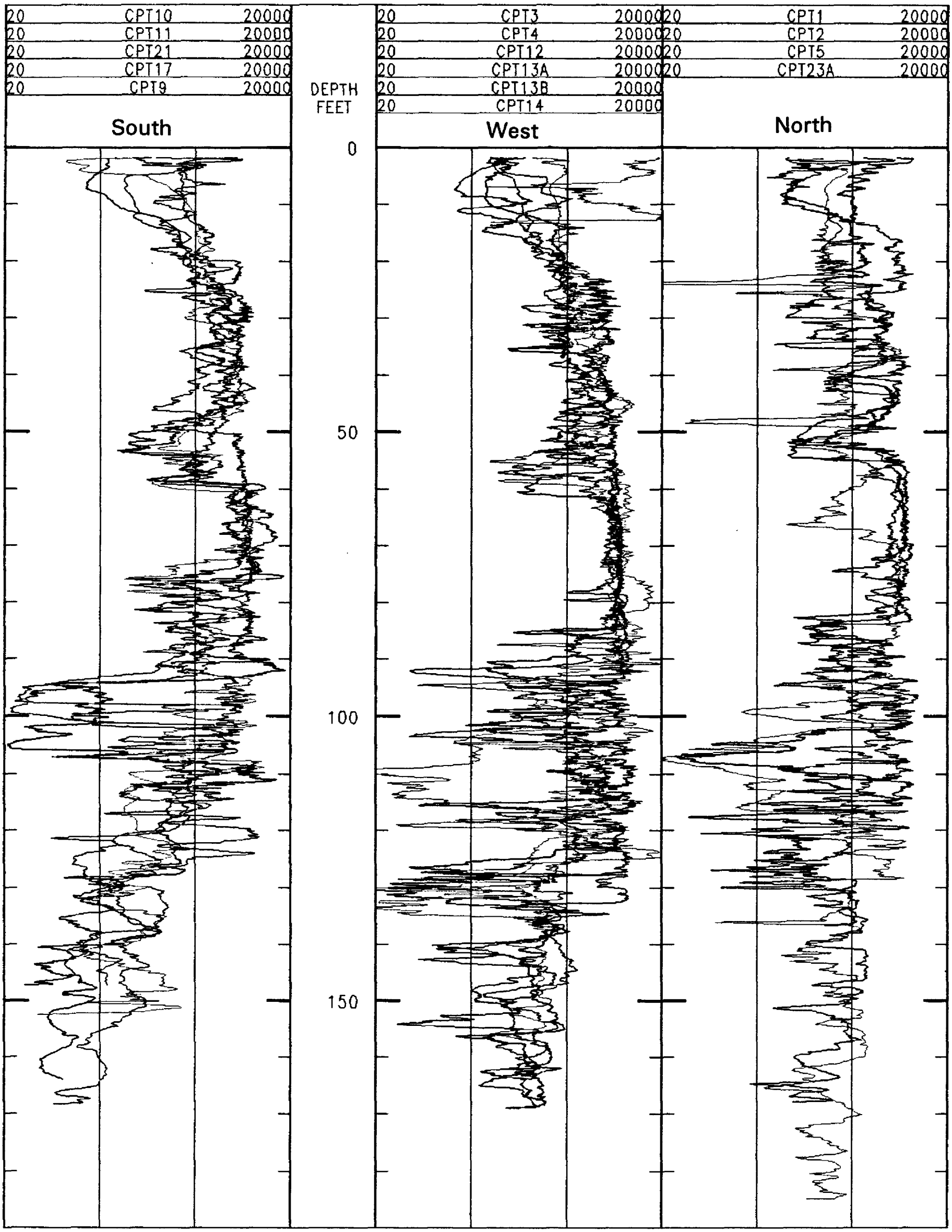

Figure 26. Resistivity logs from 15 cone penetrometer runs located south, west, and north of settling basin. Logarithmic scale ranges from 20 to 20,000 ohm-m with scale lines at 200 and 2,000 ohm-m.

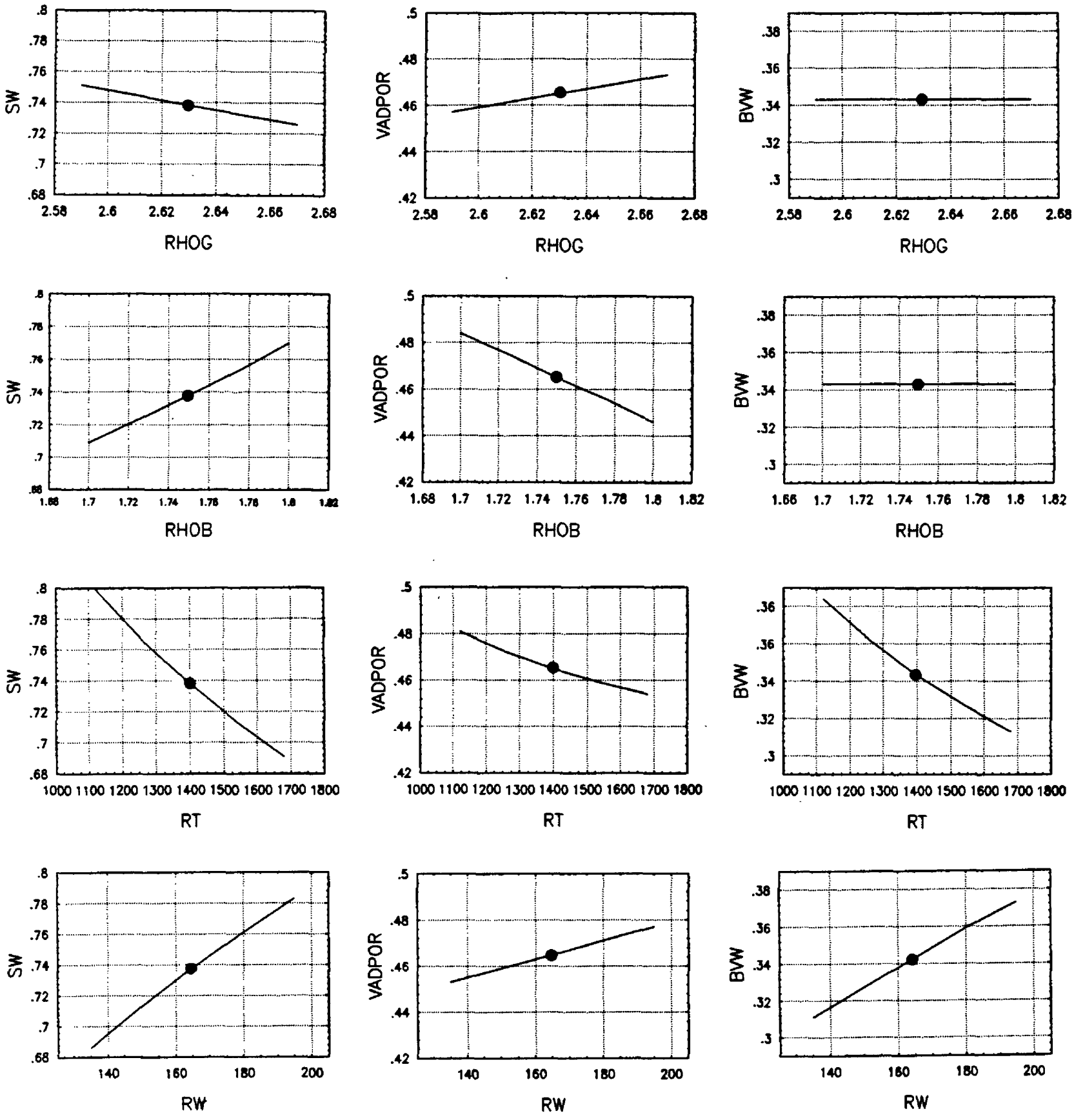

Figure 27. Sensitivity of saturation (Sw), porosity in vadose zone (Vadpor), and bulk volume water (Bvw) to changes in four parameters: grain density (Rhog), bulk density (Rhob), formation resistivity (Rt), and effective water resistivity (Rw). Values for base case (black dots) are given in the text.